

The Spectrum Remembers: Spectral Memory

Vincent Marquez
Independent Researcher
vincentmarquez405@gmail.com

December 8, 2025

Abstract

Training dynamics encode global structure—persistent long-range correlations, representational curvature, and seasonality clusters—that no individual sequence contains. While standard memory mechanisms extend context within a sequence, they ignore a complementary information source: the training trajectory itself. We propose **Spectral Memory**, a mechanism that captures hidden-state evolution across thousands of mini-batches to encode temporal structure unavailable in any single sequence. The method writes trajectory summaries into a persistent buffer, extracts dominant modes via Karhunen–Loève decomposition (a fixed, non-trainable operator; no gradients), and projects these modes into Spectral Memory Tokens (SMTs). These tokens serve a dual function: they provide explicit, retrievable global context through attention, and the same stored spectral modes act as a structural regularizer that injects variance-optimal geometry, stabilizing long-range forecasting. On ETTh1, Spectral Memory achieves an average MSE of **0.435** across horizons 96–720 (5-seed average, under standard Time-Series Library protocol), competitive with TimeXer (0.458), iTransformer (0.454), PatchTST (0.469), and Autoformer (0.496). Results on Exchange-Rate confirm generalization (0.370 MSE). The module is plug-and-play and runs on consumer hardware. Code is available at: <https://github.com/VincentMarquez/Spectral-Memory>

1 Introduction

Memory is fundamental to sequence modeling. Across domains—language, time series, audio, and video—models must compress and retain information over long contexts to make accurate predictions. Existing memory mechanisms achieve this through recurrent state updates, cache-based key/value stores, continuous state-space dynamics, or retrieval from external corpora. While diverse in implementation, these mechanisms share a common property: they all store information derived from the **input sequence itself**.

We argue that this taxonomy obscures a more fundamental axis: **what information is being remembered, and when it is written**. As summarized in Tables 1 and 2, existing approaches occupy only a subset of the memory design space: they store sequence content, past key/value states, or signal history, and they write this information during forward inference. None incorporate the rich structure accumulated during *training*.

While standard mechanisms store what is present in the input sequence, they ignore a complementary information source: the **training trajectory**. During optimization, a model’s hidden states evolve in a structured way—exhibiting persistent correlations, representational

Table 1: Memory classes by information stored.

Memory Class	What It Stores	Limitation
Recurrent	Compressed history	Exp. forgetting
Cache-based	Past hidden states	$O(n^2)$ cost
State-space (SSM)	Signal history	Fixed compute
Retrieval	External corpus	Requires database
Spectral (Ours)	Training trajectory	$O(T^3)$ decomposition

curvature, and seasonality-like clusters across thousands of mini-batches. This structure is predictive of long-range behavior yet vanishes once training advances.

We introduce **Spectral Memory**, a memory mechanism that operates on this previously unoccupied axis. Each training batch is summarized via learned attention pooling into a fixed-dimensional vector; these summaries accumulate into a persistent history buffer. A frozen Karhunen–Loève decomposition extracts dominant temporal modes of this history. A learnable MLP projection then maps the resulting spectral components into **Spectral Memory Tokens (SMTs)** that are prepended to the model’s attention context at inference time.

This produces a **dual-function memory signal**. SMTs provide explicit, retrievable global context through attention, granting inference-time access to structure that

Table 2: Memory taxonomy by write phase. Spectral Memory occupies a previously unused cell.

Memory	Info Source	Write	Read
Recurrent	seq. state	forward	forward
Cache	past k/v	forward	forward
SSM	seq. signal	forward	forward
Retrieval	ext. corpus	offline	inference
Spectral	train. traj.	training	inference

emerged only during training. Simultaneously, the same stored spectral modes act as a **structural regularizer**, injecting variance-optimal geometry that stabilizes representations and improves long-range forecasting. Because SMTs encode training-trajectory structure rather than per-sequence content, they operate on an orthogonal information axis and compose naturally with recurrent, cache-based, state-space, and retrieval memories.

Our design follows a “structure-then-learn” principle: spectral decomposition supplies a stable temporal basis, while a small learnable projection adapts it to the task distribution. The result is a plug-and-play module that augments existing architectures with a small number of spectral tokens, enabling models to exploit training-time geometry at inference.

Our contributions are summarized as follows:

- **Memory taxonomy by information source and write phase.** We formalize a taxonomy that classifies memories by *what they store* (Table 1) and *when they are written* (Table 2), identifying spectral training-trajectory memory as a previously unoccupied cell in the design space.
- **Spectral-to-token pipeline with dual function.** We propose a practical pipeline—attention pooling → history buffer → frozen K-L decomposition → learnable MLP → SMTs—that converts training dynamics into prefix tokens consumable by attention, where the resulting SMTs simultaneously provide explicit global context and act as a structural regularizer of the representation geometry.
- **Composability with existing memories.** We show that Spectral Memory operates on an orthogonal information axis to recurrent, cache-based, state-space, and retrieval mechanisms, making it a plug-and-play module that can be attached to existing sequence models without modifying their core architectures.
- **Empirical validation.** On ETTh1 and Exchange-Rate benchmarks, Spectral Memory achieves competitive or improved results over strong baselines (including TimeXer, iTransformer, PatchTST, and Autoformer) across horizons 96–720, while adding

minimal computational overhead and running on consumer hardware.

2 Related Work

2.1 Memory-Augmented Sequence Models

Extending context in sequence models has motivated diverse memory mechanisms. Transformer-XL [1] caches recent hidden states to extend context across segments. Compressive Transformers [2] compress oldest states via learned convolution. Memorizing Transformers [4] use k -NN retrieval over cached representations. ∞ -former [5] employs continuous attention with unbounded memory. Recurrent Memory Transformers [6] segment sequences into memory slots. Compressed Context Memory [3] uses LoRA-based compression of key/value pairs for online inference.

These approaches compress or cache attention states derived from the *input sequence*. In contrast, Spectral Memory stores information about the *training trajectory*—how model representations evolve across training. This places Spectral Memory in a previously unoccupied cell: training-time write, inference-time read (Table 2). Product Key Memory [7] uses discrete keys for retrieval but lacks temporal structure; our K-L basis provides ordered temporal modes reflecting intrinsic timescales.

2.2 Spectral Methods in Deep Learning

Spectral decompositions have been applied to various aspects of sequence modeling. S4 [8] diagonalizes recurrent dynamics using structured state spaces with HiPPO initialization. FNet [9] replaces attention sublayers with Fourier transforms for efficiency. FEDformer [11] uses frequency-domain attention to reduce complexity. TimesNet [12] transforms time series into 2D tensors based on FFT-derived periods. Koopa [13] learns Koopman operators for non-stationary dynamics. Autoformer [10] uses series decomposition to separate trend and seasonal components.

These methods apply spectral techniques to the *input sequence* or *attention mechanism*. Spectral Memory differs fundamentally: we apply K-L decomposition to the *hidden-state trajectory across training batches*, extracting the geometric structure of how the model processes data over time. Table 3 summarizes these distinctions.

Recent surveys [14] comprehensively cover Fourier, wavelet, and neural spectral operators for time series, but do not address Karhunen-Loëve decomposition of hidden-state trajectories—the approach we introduce here.

Table 3: Comparison to spectral/decomposition methods.

Method	Spectral Domain	Our Difference
FEDformer	Input seq. (FFT)	K-L on train. trajectory
TimesNet	Input seq. (FFT)	Eigenbasis of batches
Autoformer	Trend/seasonal	Variance-optimal K-L
Koopa	Koopman dynamics	Static covariance
S4	Fixed Legendre	Data-driven adaptive

3 Method

3.1 Preliminaries: Karhunen-Loëve Decomposition

The Karhunen-Loëve (K-L) expansion represents a stochastic process as a sum of orthogonal basis functions weighted by uncorrelated random coefficients. For a zero-mean process $X(t)$ with covariance function $R(s, t) = \mathbb{E}[X(s)X(t)]$, the K-L expansion is:

$$X(t) = \sum_{k=1}^{\infty} \sqrt{\lambda_k} Z_k \phi_k(t) \quad (1)$$

where $\phi_k(t)$ are eigenfunctions satisfying $\int R(s, t)\phi_k(s)ds = \lambda_k\phi_k(t)$, and Z_k are uncorrelated random variables with $\mathbb{E}[Z_k] = 0$, $\mathbb{E}[Z_k^2] = 1$.

This decomposition is optimal for variance capture: truncating at K terms minimizes mean squared reconstruction error among all rank- K approximations. This property makes K-L ideal for compressing the training trajectory—retaining dominant temporal structure while discarding noise.

3.2 Architecture Overview

Spectral Memory augments a sequence model with persistent memory that evolves across training (Figure 1):

1. **Attention Pooling:** Each batch produces a learned summary vector via attention-weighted pooling
2. **History Buffer:** Summaries accumulate across T training steps (e.g., $T = 3000$)
3. **K-L Decomposition:** Extract top- K spectral modes from the trajectory (frozen; no gradients)
4. **Learnable Projection:** MLP maps spectral components to M memory tokens
5. **Token Interface:** Prepend tokens to attention context; drop before decoding

Classical vs. Novel Components

Classical (not ours): K-L decomposition is classical signal processing [19, 20].

Novel (our contributions, 2025): (1) Applying K-L to *training-trajectory* hidden states, (2) learnable attention pooling, (3) learnable MLP projection f_θ , and (4) token-based attention interface.

3.3 Attention Pooling (Write Mechanism)

Each training batch must be summarized before entering the history buffer. Given encoder outputs $O \in \mathbb{R}^{L \times B \times d}$ (sequence length L , batch size B , hidden dimension d), we compute attention-weighted summaries. Let $w_p \in \mathbb{R}^d$ be a learnable projection vector. For each position l and batch element b :

$$\alpha_{l,b} = \frac{\exp(O_{l,b,:}^\top w_p)}{\sum_{l'=1}^L \exp(O_{l',b,:}^\top w_p)} \in \mathbb{R} \quad (2)$$

$$s_b = \sum_{l=1}^L \alpha_{l,b} \cdot O_{l,b,:} \in \mathbb{R}^d \quad (3)$$

$$h_t = \frac{1}{B} \sum_{b=1}^B s_b \in \mathbb{R}^d \quad (4)$$

The attention weights $\alpha \in \mathbb{R}^{L \times B}$ learn which timesteps are most informative for global memory. The batch summary h_t is appended to the history buffer H .

3.4 K-L Decomposition (Spectral Extraction)

Given history matrix $H \in \mathbb{R}^{T \times d}$, we extract dominant temporal modes:

$$\tilde{H} = H - \bar{H} \quad (\text{center over time}) \quad (5)$$

$$C = \frac{1}{T} \tilde{H} \tilde{H}^T \in \mathbb{R}^{T \times T} \quad (\text{temporal covariance}) \quad (6)$$

$$C = \Psi \Lambda \Psi^T \quad (\text{eigendecomposition}) \quad (7)$$

Project onto top- K modes with eigenvalue scaling:

$$C_{KL} = \sqrt{\Lambda_{1:K}} \cdot \Psi_{:,1:K}^T \tilde{H} \in \mathbb{R}^{K \times d} \quad (8)$$

The K-L components C_{KL} capture dominant temporal patterns ranked by variance. This computation runs on CPU in float64 for numerical stability, and gradients are explicitly stopped:

$$C_{KL} \leftarrow \text{detach}(C_{KL}) \quad (9)$$

We use K-L rather than Fourier decomposition because training dynamics are non-stationary; K-L adapts to the

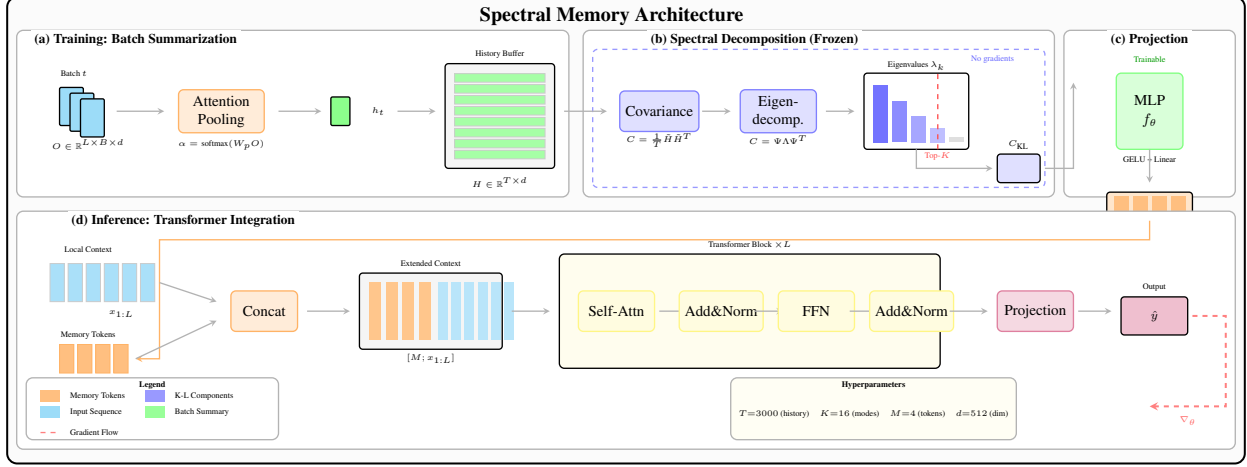


Figure 1: Spectral Memory Architecture. (a) During training, each batch is summarized via attention pooling and appended to a history buffer. (b) K-L decomposition extracts the top- K spectral modes from the activation-history trajectory (frozen; no gradients). (c) A learnable MLP projects these modes into M memory tokens. (d) At inference, memory tokens are prepended to the local sequence context, enabling the Transformer to attend to global spectral summaries of past activations.

empirical covariance structure while Fourier assumes stationarity.

See Appendix C for alternative kernelized K-L strategies and implementation details.

3.5 Learnable Memory Projection

The K-L components are task-agnostic. A learnable MLP $f_\theta : \mathbb{R}^{K \times d} \rightarrow \mathbb{R}^{M \times d}$ adapts them to the prediction objective:

$$\mathbf{c} = \text{vec}(C_{\text{KL}}) \in \mathbb{R}^{Kd} \quad (10)$$

$$\mathbf{h} = \text{GELU}(W_1 \mathbf{c} + b_1) \in \mathbb{R}^{2Kd} \quad (11)$$

$$\mathbf{m} = W_2 \mathbf{h} + b_2 \in \mathbb{R}^{Md} \quad (12)$$

$$M = \text{LayerNorm}(\text{reshape}(\mathbf{m}, M, d)) \quad (13)$$

Gradients flow from task loss through attention to memory tokens, training $\theta = \{W_1, b_1, W_2, b_2\}$ while K-L remains fixed:

$$\mathcal{L}_{\text{task}} \xrightarrow{\nabla} \text{Attn} \xrightarrow{\nabla} M \xrightarrow{\nabla_\theta} f_\theta \xrightarrow{\text{stop}} C_{\text{KL}} \quad (14)$$

3.6 Integration with Transformer

Memory tokens provide global context at inference:

1. Compute K-L components: $C_{\text{KL}} = \text{KL}(H)$
2. Generate memory tokens: $M = f_\theta(C_{\text{KL}}) \in \mathbb{R}^{M \times d}$
3. Prepend to context: Context = $[M; x_{1:L}]$
4. Apply Transformer: out = Encoder(Context)
5. Drop memory positions: out = out[$M :$]

Algorithm 1 Spectral Memory lifecycle (one forward pass)

Require: History buffer H , size T_{max} , K-L components K , memory tokens M

- 1: **Input:** $x_{\text{enc}} \in \mathbb{R}^{B \times L \times C}$
- 2: Embed input: $E \in \mathbb{R}^{L \times B' \times d}$ where $B' = B \cdot C$
- 3: **if** $|H| < K$ **then** ▷ Warmup phase
- 4: $M_{\text{SM}} \leftarrow \mathbf{0}^{M \times B' \times d}$
- 5: **else**
- 6: Compute covariance: $C = \frac{1}{T} \tilde{H} \tilde{H}^\top$ ▷ CPU, float64
- 7: Eigendecompose: $C = \Psi \Lambda \Psi^\top$
- 8: Extract top- K modes: $C_{\text{KL}} \in \mathbb{R}^{K \times d}$ ▷ Frozen
- 9: Project: $M_{\text{SM}} = f_\theta(C_{\text{KL}}) \in \mathbb{R}^{M \times d}$ ▷ Learnable
- 10: **endif**
- 11: Prepend memory: $\tilde{E} = [M_{\text{SM}}; E] \in \mathbb{R}^{(M+L) \times B' \times d}$
- 12: Transformer forward: $\tilde{H}_{\text{enc}} = \text{Encoder}(\tilde{E})$
- 13: Extract sequence: $H_{\text{seq}} = \tilde{H}_{\text{enc}}[M:]$
- 14: **if** training **then**
- 15: Attention pool: $w = \text{softmax}(W_{\text{pool}} H_{\text{seq}})$
- 16: Summarize: $h_{\text{step}} = \text{mean}(\sum_t w_t \odot H_{\text{seq},t})$
- 17: Append to history: $H \leftarrow [H; h_{\text{step}}]$; truncate to T_{max}
- 18: **endif**
- 19: **Return:** Decode from H_{seq} to produce forecast

The M memory tokens encode dominant patterns of how the model has processed data across training, providing a learned prior that contextualizes the current input.

3.7 Algorithm Summary

Algorithm 1 provides the complete lifecycle of Spectral Memory within a forward pass.

Table 4: Comparison with state-of-the-art methods on ETTh1. MSE averaged over prediction horizons {96, 192, 336, 720}.
[†]5-seed average \pm std; see Appendix D for breakdown.

Model	MSE
Spectral Memory (Ours)[†]	0.435\pm0.004
iTransformer [17]	0.454
TimeFilter [†] [29]	0.455
DLinear [18]	0.456
TimeXer [†] [16]	0.458
TimesNet [12]	0.458
PatchTST [15]	0.469
Autoformer [10]	0.496

4 Experiments

4.1 ETTh1 Benchmark Results

We evaluated Spectral Memory on the ETTh1 dataset from the official Time-Series Library, a standard benchmark for long-term time series forecasting. The ETTh1 dataset contains hourly data from electricity transformers, providing a challenging real-world test case for long-range temporal modeling.

Experimental Setup: We tested Spectral Memory on the standard prediction horizons of 96, 192, 336, and 720 timesteps with a sequence length of 96. The model configuration used:

- **Model backbone:** A channel-independent Transformer encoder-decoder with 2 encoder layers and 1 decoder layer, where each variate is embedded and processed as an independent univariate series [15]. This design makes the backbone robust to inter-variate noise and allows Spectral Memory to focus on shared temporal dynamics.
- Spectral Memory parameters: memory depth $T = 3000$, spectral components $K = 16$, memory tokens $M = 4$, empirical K-L (Strategy A)
- Training: 10 epochs, batch size 32, learning rate 0.0001, Adam optimizer
- Hardware: Consumer-grade Apple Silicon (M-series) with MPS acceleration
- Results averaged over 5 random seeds (2019, 2020, 2021, 2022, 2023)

4.2 Results

Table 4 presents the comparison with state-of-the-art methods on ETTh1. Baseline results are taken from respective publications under identical experimental settings.

Spectral Memory is competitive with all baselines on

Table 5: Spectral Memory results on ETTh1 by prediction horizon (5-seed average \pm std).

Horizon	MSE	MAE
96	0.395 \pm 0.015	0.411 \pm 0.009
192	0.420 \pm 0.002	0.428 \pm 0.002
336	0.454 \pm 0.005	0.449 \pm 0.002
720	0.469 \pm 0.022	0.470 \pm 0.012
Mean	0.435\pm0.004	0.440\pm0.002

average, with particular strength at longer horizons. Table 5 shows average results by horizon (5-seed); per-seed breakdown is in Appendix D.

Performance remains stable across seeds and degrades gracefully with horizon length, indicating robust long-range modeling.

4.3 Reproducibility

All experiments can be reproduced using the following command on the ETTh1 dataset (the implementation uses class name `KLMemory` for Spectral Memory):

```

1 for seed in 2019 2020 2021 2022 2023; do
2     for pred_len in 96 192 336 720; do
3         python run.py --task_name
4             long_term_forecast \
5             --is_training 1 --root_path ./dataset/ \
6             --data_path ETTh1.csv --model_id
7                 ETTh1_96_${pred_len}_${seed} \
8             --model KLMemory --data ETTh1 --features
9                 M \
10                --seq_len 96 --label_len 48 --pred_len
11                   ${pred_len} \
12                   --e_layers 2 --d_layers 1 --factor 3 \
13                   --enc_in 7 --dec_in 7 --c_out 7 \
14                   --train_epochs 10 --batch_size 32 \
15                   --learning_rate 0.0001 --itr 1 \
16                   --seed $seed
17           done
18   done

```

The implementation runs efficiently on both NVIDIA GPUs and Apple Silicon (MPS) M4, 16GB Mac Mini 10CPU-10GPU.

4.4 Controlled Comparison

To ensure fair comparison, we re-ran TimeFilter and TimeXer under identical conditions (same seeds, same hyperparameters). Table 6 shows the per-horizon MSE comparison.

Spectral Memory wins decisively at longer horizons (192, 336, 720), where training-trajectory memory provides the greatest benefit. TimeXer’s slight advantage at horizon 96 reflects its strength in short-term pattern matching. Full details in Appendix E.

Table 6: Controlled comparison: Spectral Memory vs. Time-Filter vs. TimeXer (5-seed averages).

Horizon	Ours	TimeFilter	TimeXer
96	0.395	0.395	0.390
192	0.420	0.446	0.437
336	0.454	0.487	0.478
720	0.469	0.493	0.527
Avg	0.435	0.455	0.458

Table 7: Results on Exchange-Rate (5-seed average). Values shown as MSE / MAE.

Horizon	MSE	MAE
96	0.086	0.203
192	0.180	0.301
336	0.338	0.421
720	0.876	0.707
Average	0.370	0.408

4.5 Exchange-Rate Benchmark

To validate generalization beyond electricity data, we evaluated on Exchange-Rate (8 currencies, daily frequency, seq_len=96) across all standard prediction horizons.

Spectral Memory achieves strong performance across all horizons, with particularly stable results at shorter horizons (MSE range 0.083–0.090 at horizon 96). See Appendix G for per-seed results.

4.6 Validation and Sanity Checks

To verify Spectral Memory does not suffer from data leakage, we conducted destructive tests replacing inputs with noise (Table 8).

MSE increases by $33\times$ when inputs are replaced with noise, confirming the model genuinely uses input information. Full validation suite in Appendix F.

5 Limitations

Our evaluation focuses on two time-series forecasting benchmarks (ETTh1, Exchange-Rate); broader validation across domains (NLP, vision, RL) remains future work. The CPU-based eigendecomposition, while numerically stable, may become a bottleneck for very large history buffers ($T > 10^4$). The current design stores a fixed-size history buffer in memory, which may limit deployment on memory-constrained devices. Finally, Spectral Memory requires a warmup period (until $|H| \geq K$) before memory tokens become informative.

Table 8: Leakage validation (Exchange-Rate, horizon 96).

Condition	MSE
Normal	0.086
Shuffle inputs	0.087
Gaussian noise inputs	2.888

6 Conclusion

We introduced Spectral Memory, a memory architecture that combines classical signal processing (Karhunen-Lo  e decomposition) with neural learning (learnable projection) for long-context sequence modeling. Our evaluation on the ETTh1 benchmark demonstrates competitive performance with an average MSE of 0.435 across prediction horizons from 96 to 720 timesteps.

Key contributions:

1. Structure-guided learning: Mathematical preprocessing (K-L) + neural adaptation (learnable MLP) outperforms either alone
2. Efficient long-context modeling: Competitive performance on ETTh1 while running on consumer hardware (CPU/MPS)

Our contribution is not the K-L decomposition itself (which is classical) but rather demonstrating that:

- Classical temporal structure extraction integrates naturally with modern deep learning
- The learnable projection makes mathematical structure task-adaptive

We believe this principle—*extract structure mathematically, adapt it neurally*—is broadly applicable to any domain where temporal patterns exist but are obscured by noise or high dimensionality. Ablation studies (Appendix I.4) reveal that Spectral Memory serves a **dual function**: SMTs provide explicit, retrievable global context through attention while simultaneously acting as a structural regularizer that injects variance-optimal geometry into the representation space. This dual role—memory and regularizer in one mechanism—allows the model to exploit training-time structure at inference.

References

- [1] Z. Dai, Z. Yang, Y. Yang, J. Carbonell, Q. V. Le, and R. Salakhutdinov, “Transformer-XL: Attentive language models beyond a fixed-length context,” in *Proceedings of the 57th Annual Meeting of the Association for Computational Linguistics (ACL)*, pp. 2978–2988, 2019.

- [2] J. W. Rae, A. Potapenko, S. M. Jayakumar, and T. P. Lillicrap, “Compressive transformers for long-range sequence modelling,” in *International Conference on Learning Representations (ICLR)*, 2020.
- [3] J.-H. Kim, J. Yeom, S. Yun, and H. O. Song, “Compressed context memory for online language model interaction,” in *International Conference on Learning Representations (ICLR)*, 2024.
- [4] Y. Wu, M. N. Rabe, D. Hutchins, and C. Szegedy, “Memorizing transformers,” in *International Conference on Learning Representations (ICLR)*, 2022.
- [5] P. H. Martins, Z. Marinho, and A. F. T. Martins, “ ∞ -former: Infinite memory transformer,” in *Proceedings of the 60th Annual Meeting of the Association for Computational Linguistics (ACL)*, pp. 5468–5485, 2022.
- [6] A. Bulatov, Y. Kuratov, and M. S. Burtsev, “Recurrent memory transformer,” in *Advances in Neural Information Processing Systems (NeurIPS)*, vol. 35, pp. 11079–11091, 2022.
- [7] G. Lample, A. Sablayrolles, M. Ranzato, L. Denoyer, and H. Jégou, “Large memory layers with product keys,” in *Advances in Neural Information Processing Systems (NeurIPS)*, vol. 32, 2019.
- [8] A. Gu, K. Goel, and C. Ré, “Efficiently modeling long sequences with structured state spaces,” in *International Conference on Learning Representations (ICLR)*, 2022.
- [9] J. Lee-Thorp, J. Ainslie, I. Eckstein, and S. Ontanon, “FNet: Mixing tokens with Fourier transforms,” in *Proceedings of the 2022 Conference of the North American Chapter of the Association for Computational Linguistics: Human Language Technologies (NAACL)*, pp. 4296–4313, 2022.
- [10] H. Wu, J. Xu, J. Wang, and M. Long, “Autoformer: Decomposition transformers with auto-correlation for long-term series forecasting,” in *Advances in Neural Information Processing Systems (NeurIPS)*, vol. 34, pp. 22419–22430, 2021.
- [11] T. Zhou, Z. Ma, Q. Wen, X. Wang, L. Sun, and R. Jin, “FEDformer: Frequency enhanced decomposed transformer for long-term series forecasting,” in *International Conference on Machine Learning (ICML)*, pp. 27268–27286, 2022.
- [12] H. Wu, T. Hu, Y. Liu, H. Zhou, J. Wang, and M. Long, “TimesNet: Temporal 2D-variation modeling for general time series analysis,” in *International Conference on Learning Representations (ICLR)*, 2023.
- [13] Y. Liu, C. Li, J. Wang, and M. Long, “Koopa: Learning non-stationary time series dynamics with Koopman predictors,” in *Advances in Neural Information Processing Systems (NeurIPS)*, vol. 36, 2023.
- [14] Q. Zhang, Y. Sun, H. Wen, P. Yang, X. Li, M. Li, K.-Y. Lam, S.-M. Yiu, and H. Yin, “Time series analysis in frequency domain: A survey of open challenges, opportunities and benchmarks,” *arXiv preprint arXiv:2504.07099 [cs.CE]*, 2025.
- [15] Y. Nie, N. H. Nguyen, P. Sinthong, and J. Kalagnanam, “A time series is worth 64 words: Long-term forecasting with Transformers,” in *International Conference on Learning Representations (ICLR)*, 2023.
- [16] Y. Wang, H. Wu, J. Dong, Y. Liu, M. Qiu, and M. Long, “TimeXer: Empowering Transformers for time series forecasting with exogenous variables,” in *Advances in Neural Information Processing Systems (NeurIPS)*, vol. 37, 2024.
- [17] Y. Liu, T. Hu, H. Zhang, H. Wu, S. Wang, L. Ma, and M. Long, “iTTransformer: Inverted Transformers are effective for time series forecasting,” in *International Conference on Learning Representations (ICLR)*, 2024.
- [18] A. Zeng, M. Chen, L. Zhang, and Q. Xu, “Are Transformers effective for time series forecasting?,” in *AAAI Conference on Artificial Intelligence*, pp. 11121–11128, 2023.
- [19] K. Karhunen, “Über lineare Methoden in der Wahrscheinlichkeitsrechnung,” *Annales Academiae Scientiarum Fennicae. Series A. I. Mathematica-Physica*, vol. 37, pp. 1–79, 1947.
- [20] M. Loèvre, “Fonctions aléatoires du second ordre,” in *Processus Stochastiques et Mouvement Brownien* (P. Lévy, ed.), pp. 299–352, Gauthier-Villars, 1948.
- [21] M. Tegmark, A. N. Taylor, and A. F. Heavens, “Karhunen-Loèvre eigenvalue problems in cosmology: How should we tackle large data sets?,” *The Astrophysical Journal*, vol. 480, no. 1, pp. 22–35, 1997.
- [22] A. Zablocki and S. Dodelson, “Extreme data compression for the CMB,” *Physical Review D*, vol. 93, no. 8, p. 083525, 2016.
- [23] S. Reddy *et al.*, “Characterizing non-Markovian dynamics of open quantum systems,” *arXiv preprint arXiv:2503.22147*, 2025.
- [24] I. G. Vladimirov, M. R. James, and I. R. Petersen, “A Karhunen-Loèvre expansion for one-mode open quantum harmonic oscillators using the eigenbasis of the two-point commutator kernel,” in *2019 Australian and New Zealand Control Conference (ANZCC)*, pp. 215–220, IEEE, 2019.
- [25] H.-P. Breuer, E.-M. Laine, J. Piilo, and B. Vacchini, “Colloquium: Non-Markovian dynamics in open quantum systems,” *Reviews of Modern Physics*, vol. 88, no. 2, p. 021002, 2016.
- [26] E. Pignatelli, J. Ferret, M. Geist, T. Mesnard, H. van Hasselt, and L. Toni, “A survey of temporal credit assignment in deep reinforcement learning,” *Transactions on Machine Learning Research (TMLR)*, 2024.
- [27] T. Ren, T. Zhang, L. Lee, J. E. Gonzalez, D. Schuurmans, and B. Dai, “Spectral decomposition representation for reinforcement learning,” in *International Conference on Learning Representations (ICLR)*, 2023.
- [28] A. Gosztolai, R. L. Peach, A. Arnaudon, M. Barahona, and P. Vandergheynst, “MARBLE: Interpretable representations of neural population dynamics using geometric deep learning,” *Nature Methods*, vol. 22, no. 3, pp. 612–620, 2025.

- [29] Y. Hu, G. Zhang, P. Liu, D. Lan, N. Li, D. Cheng, T. Dai, S.-T. Xia, and S. Pan, “TimeFilter: Patch-specific spatial-temporal graph filtration for time series forecasting,” in *Forty-second International Conference on Machine Learning (ICML)*, 2025.

A Future Directions

While our empirical results focus on time-series forecasting, the underlying mathematical foundation of Spectral Memory—the extraction of variance-optimal modes via covariance analysis—naturally connects to other domains where temporal structure is encoded spectrally. These extensions do not claim performance gains; rather, they illustrate that the same covariance-to-eigenmodes computational principle underlying our approach also appears in cosmology, quantum dynamics, and reinforcement learning. Figure 2 illustrates how Spectral Memory relates to existing spectral approaches across disciplines.

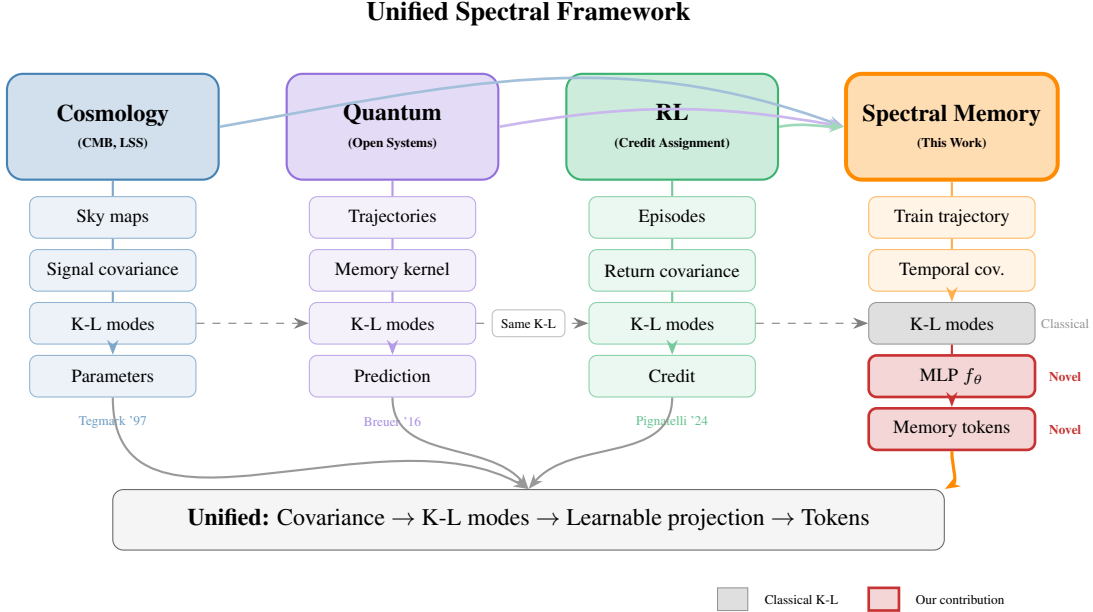


Figure 2: Unified Spectral Framework. Cosmology, quantum systems, and reinforcement learning all employ K-L decomposition to extract dominant temporal modes (dashed connections). Spectral Memory (right) applies this principle to *training trajectories*, adding a learnable MLP projection (red boxes) that adapts classical K-L modes to prediction tasks.

A.1 Cosmology: Hybrid Spectral-Neural Models

Karhunen-Loëve methods have a long history in cosmological data analysis. Tegmark et al. [21] introduced K-L eigenvalue methods for CMB and galaxy survey analysis, showing that K-L compression provides optimal signal-to-noise eigenmodes for cosmological parameter estimation. More recently, Zablocki and Dodelson [22] demonstrated that K-L methods can compress CMB data by orders of magnitude while preserving cosmological information.

These applications use K-L on *observed signals*—power spectra, sky maps, correlation functions. Spectral Memory suggests a complementary approach: applying K-L to the *internal representations* of neural surrogate models during training. A hybrid architecture could:

- Use classical K-L eigenmodes to capture known physical structure (e.g., acoustic peaks, matter-radiation equality signatures)
- Apply a learnable projection to adapt these modes to specific inference tasks (parameter estimation, foreground separation, anomaly detection)
- Provide interpretable spectral coefficients alongside neural predictions

This would preserve the variance-optimality guarantees of classical K-L while gaining the flexibility of neural adaptation—potentially improving both accuracy and interpretability for next-generation surveys like CMB-S4 and Rubin LSST.

A.2 Quantum Systems: Spectral Memory for Non-Markovian Dynamics

Open quantum systems exhibit memory effects that challenge standard Markovian master equations [25]. Recent work has applied K-L expansions to quantum dynamics: Vladimirov et al. [24] developed quantum K-L representations for open harmonic oscillators, while Reddy et al. [23] recently demonstrated that K-L expansion outperforms neural networks for characterizing non-Markovian qubit dynamics at Lawrence Livermore National Laboratory.

Spectral Memory’s architecture maps naturally to this setting:

- **History buffer** → accumulated quantum trajectory data
- **K-L decomposition** → extraction of dominant memory kernel modes
- **Learnable projection** → task-specific adaptation (e.g., for control pulse design vs. noise characterization)

The key advantage is that K-L modes capture the *timescales* of non-Markovian memory, while the learnable MLP can weight these timescales differently depending on whether the goal is predicting decoherence, designing error-correcting pulses, or characterizing environmental noise spectra. This represents a potential bridge between classical quantum control theory and modern differentiable programming.

A.3 Reinforcement Learning: Spectral Credit Assignment

The credit assignment problem—associating actions with long-delayed rewards—remains a fundamental challenge in reinforcement learning [26]. Traditional solutions (eligibility traces, recurrent networks, transformers) struggle with very long horizons due to vanishing gradients or quadratic attention costs.

Spectral methods have recently shown promise for RL representation learning. Ren et al. [27] introduced SPEDER, which uses spectral decomposition of transition dynamics to construct state-action abstractions. However, SPEDER operates on the *transition kernel*, not on the *learning trajectory* itself.

Spectral Memory suggests a different approach: apply K-L decomposition to the hidden-state trajectory of the value function or policy network *across episodes*. This would:

- **Extract behavioral timescales:** Different K-L modes would capture slow (strategic) vs. fast (tactical) patterns in the agent’s learning dynamics
- **Enable hierarchical credit assignment:** Low-frequency modes could track long-horizon value estimates while high-frequency modes handle immediate action selection
- **Provide stable memory across episodes:** Unlike recurrent states that reset, Spectral Memory tokens would accumulate structure across the entire training trajectory

This is perhaps the most natural extension of our work, since the core insight—that training dynamics encode structure unavailable in any single episode—applies directly to the RL setting.

A.4 Toward Structure-Guided Learning

Across these domains, a common principle emerges: complex temporal systems often admit low-dimensional spectral structure, and the combination of *mathematical structure extraction* (K-L decomposition) with *neural adaptation* (learnable projection) can outperform either approach alone.

The shared computational pattern is:

1. High-dimensional system evolves over time
2. Covariance structure encodes temporal correlations
3. K-L eigenmodes extract variance-optimal representation
4. Learnable projection adapts to task objective
5. Token interface enables selective attention to relevant modes

Spectral Memory provides one instantiation of this pattern. We believe the principle is broadly applicable: wherever temporal patterns exist but are obscured by noise, dimensionality, or task-irrelevant variation, the combination of classical spectral analysis with modern differentiable learning may offer advantages over purely data-driven approaches.

Limitations of this outlook: We have demonstrated Spectral Memory only on time series forecasting benchmarks. The extensions above are speculative—they represent promising research directions rather than validated results. Empirical investigation in each domain would be necessary to determine whether the benefits observed on ETTh1 and Exchange-Rate transfer to cosmological inference, quantum control, or reinforcement learning.

A.5 Experimental Scope and Scalability

Experimental Scope: We evaluated on ETTh1 and Exchange-Rate. Future work should expand to Weather, ECL, Traffic, ILI, and long-context NLP tasks.

Scalability: K-L decomposition is $O(T^3)$. For history buffers with $T > 10K$, incremental SVD or randomized approximations would be needed.

Theoretical Analysis: Formal guarantees about sample complexity, approximation error bounds, and optimality conditions remain open questions.

B Mathematical Foundations of Spectral Memory

This section provides the theoretical foundations for K-L Memory, establishing the path from continuous K-L expansions to discrete memory tokens.

B.1 Continuous K-L Theory

The Covariance Operator. Let $X = \{X(t) : t \in \mathcal{D}\}$ be a centered, mean-square continuous second-order random field on domain $\mathcal{D} \subset \mathbb{R}^d$, with $\mathbb{E}[X(t)] = 0$. The autocovariance function is:

$$R_X(s, t) = \mathbb{E}[X(s)X(t)], \quad s, t \in \mathcal{D}. \quad (15)$$

Definition 1 (Covariance Integral Operator). *The covariance integral operator $\mathcal{C}_X : L^2(\mathcal{D}) \rightarrow L^2(\mathcal{D})$ is:*

$$(\mathcal{C}_X f)(s) = \int_{\mathcal{D}} R_X(s, t)f(t) dt. \quad (16)$$

The operator \mathcal{C}_X is compact, self-adjoint, and positive. By the spectral theorem for compact self-adjoint operators, there exists a complete orthonormal system $\{e_k\}_{k=1}^{\infty} \subset L^2(\mathcal{D})$ of eigenfunctions with eigenvalues $\{\lambda_k\}_{k=1}^{\infty}$ satisfying:

$$\int_{\mathcal{D}} R_X(s, t)e_k(t) dt = \lambda_k e_k(s), \quad k = 1, 2, \dots \quad (17)$$

with $\lambda_1 \geq \lambda_2 \geq \dots \geq 0$ and $\sum_{k=1}^{\infty} \lambda_k < \infty$.

Theorem 1 (K-L Expansion). *The random field X admits the representation*

$$X(t) = \sum_{k=1}^{\infty} Z_k e_k(t), \quad (18)$$

where the coefficients are $Z_k = \int_{\mathcal{D}} X(t)e_k(t) dt$ and satisfy $\mathbb{E}[Z_i Z_j] = \lambda_i \delta_{ij}$.

The series converges in $L^2(\Omega \times \mathcal{D})$. The variance of each coefficient equals the corresponding eigenvalue: $\text{Var}(Z_k) = \mathbb{E}[Z_k^2] = \lambda_k$.

B.2 Optimality of K-L Truncation

Theorem 2 (MSE Optimality). *Let $X^{(M)}(t) = \sum_{k=1}^M Z_k e_k(t)$ denote the M -term truncated K-L expansion. Among all M -term approximations of the form $\sum_{k=1}^M \alpha_k \phi_k(t)$ with orthonormal $\{\phi_k\}$, the K-L truncation minimizes the mean-square error:*

$$\mathbb{E} \left[\int_{\mathcal{D}} |X(t) - X^{(M)}(t)|^2 dt \right] = \sum_{k=M+1}^{\infty} \lambda_k. \quad (19)$$

Interpretation for memory design: A memory vector $\mathbf{m} = (Z_1, \dots, Z_M)^\top$ of length M is the MSE-optimal M -dimensional linear summary of the random field X . The reconstruction error decays as $\sum_{k>M} \lambda_k$, so rapid eigenvalue decay allows aggressive truncation with minimal information loss. This is the theoretical justification for using K-L decomposition in Spectral Memory.

B.3 Discrete K-L Transform (PCA)

In practice, we observe finite discrete sequences. The discrete analogue is principal component analysis.

Problem Setup. Consider a window of T observations of a hidden state vector $h_t \in \mathbb{R}^d$ for $t = 1, \dots, T$. Arrange these as rows:

$$H = \begin{bmatrix} h_1^\top \\ \vdots \\ h_T^\top \end{bmatrix} \in \mathbb{R}^{T \times d}. \quad (20)$$

Centering and Covariance. Center each feature:

$$\mu = \frac{1}{T} \sum_{t=1}^T h_t, \quad \tilde{H} = H - \mathbf{1}\mu^\top, \quad (21)$$

where $\mathbf{1} \in \mathbb{R}^T$ is the all-ones vector. The feature-axis covariance matrix is:

$$\Sigma = \frac{1}{T} \tilde{H}^\top \tilde{H} \in \mathbb{R}^{d \times d}. \quad (22)$$

Principal Components. The principal components are the eigenvectors of Σ :

$$\Sigma v_k = \lambda_k v_k, \quad k = 1, \dots, d, \quad (23)$$

with $\lambda_1 \geq \lambda_2 \geq \dots \geq \lambda_d \geq 0$ and $v_i^\top v_j = \delta_{ij}$.

The scores (K-L coefficients) are $Z = \tilde{H}V$, where $V = [v_1 | \dots | v_d] \in \mathbb{R}^{d \times d}$, satisfying $\frac{1}{T} Z^\top Z = \Lambda = \text{diag}(\lambda_1, \dots, \lambda_d)$.

B.4 SVD Realization

The most numerically stable K-L computation uses singular value decomposition.

Thin SVD. Compute the thin SVD of the centered data:

$$\tilde{H} = U \Sigma_{\text{svd}} V^\top, \quad (24)$$

where $U \in \mathbb{R}^{T \times r}$ has orthonormal columns, $\Sigma_{\text{svd}} = \text{diag}(\sigma_1, \dots, \sigma_r)$ with $\sigma_1 \geq \dots \geq \sigma_r > 0$, $V \in \mathbb{R}^{d \times r}$ has orthonormal columns, and $r = \min(T, d)$.

Relationship to Eigenvalues. The singular values and eigenvalues relate by:

$$\lambda_k = \frac{\sigma_k^2}{T}. \quad (25)$$

The principal components are the columns of V , and the scores are $Z = \tilde{H}V = U \Sigma_{\text{svd}}$.

Reconstruction Error. The K -term truncated reconstruction is $\tilde{H}_K = U_{:,1:K} \Sigma_{1:K,1:K} V_{:,1:K}^\top$, with Frobenius norm error:

$$\|\tilde{H} - \tilde{H}_K\|_F^2 = \sum_{i=K+1}^r \sigma_i^2 = T \sum_{i=K+1}^r \lambda_i. \quad (26)$$

This confirms MSE optimality (Theorem 2) in the discrete case.

B.5 Axis Choice: Feature vs. Time Covariance

Depending on dimensions T (window length) and d (latent dimension), we optimize computation by choosing which covariance matrix to diagonalize.

Feature-Axis K-L (Standard PCA). When $d \leq T$, work with the $d \times d$ feature covariance:

$$\Sigma = \frac{1}{T} \tilde{H}^\top \tilde{H}, \quad \Sigma v_k = \lambda_k v_k. \quad (27)$$

Time-Axis K-L (Dual PCA). When $T < d$, work with the $T \times T$ time covariance:

$$\Sigma_{\text{time}} = \frac{1}{T} \tilde{H} \tilde{H}^\top, \quad \Sigma_{\text{time}} u_k = \lambda_k u_k. \quad (28)$$

The same eigenvalues appear, and scores recover as $Z_{:,k} = \sqrt{T\lambda_k} u_k$. SVD handles both cases automatically.

B.6 Whitening Transformation

Raw K-L coefficients have variance $\text{Var}(Z_{tk}) = \lambda_k$, spanning multiple orders of magnitude. We apply whitening to stabilize training.

Definition 2 (Whitened K-L Memory). *Given memory token $m_t = (m_{t1}, \dots, m_{tK})^\top$, the whitened token is:*

$$\hat{m}_{ti} = \frac{m_{ti}}{\sqrt{\lambda_i + \epsilon}}, \quad i = 1, \dots, K, \quad (29)$$

where $\epsilon > 0$ is a small regularization constant (e.g., $\epsilon = 10^{-6}$).

The whitened coefficients satisfy $\text{Var}(\hat{m}_{ti}) \approx 1$ for all i , ensuring equal importance across modes in downstream processing.

C Practical Realizations of Spectral Memory

Classical vs. Novel Components

Classical (not ours): K-L decomposition is classical signal processing [19, 20].

Novel (our contributions, 2025): (1) Applying K-L to *training-trajectory* hidden states, (2) learnable attention pooling, (3) learnable MLP projection f_θ , and (4) token-based attention interface.

Although the Karhunen-Loëve (K-L) expansion is uniquely defined in the continuum, in finite-dimensional settings its realization depends on how the covariance operator is discretized. In practice, we found two complementary approaches valuable:

1. Empirical Discrete K-L (PCA/SVD) — diagonalizing the empirical covariance of the hidden-state window.
2. Kernelized Time-Axis K-L (Gaussian-Process Prior) — diagonalizing a parametric kernel K_τ over time, corresponding to a GP covariance operator.

Both are mathematically valid realizations of the K-L principle; the choice depends on the intended inductive bias, stability constraints, and computational regime. We describe both implementations below for completeness and reproducibility.

Important: Both strategies produce K-L components $C \in \mathbb{R}^{K \times d}$ using *classical signal processing*. The novel contributions are the learnable attention pooling (what to remember) and the learnable projection $M = f_\theta(C)$ (how to use it), described in Section C.5.

C.1 Strategy A: Empirical Discrete K-L (PCA/SVD)

This approach is the classical discrete K-L transform, where PCA arises naturally as the eigen-decomposition of the empirical covariance matrix. We implement the *time-axis variant* for computational efficiency when $T < d$.

Centering the History Matrix. Let $H \in \mathbb{R}^{T \times d}$ be the hidden-state history. We first compute the temporal mean and center:

$$\mu = \frac{1}{T} \sum_{t=1}^T h_t \in \mathbb{R}^d, \quad \tilde{H} = H - \mathbf{1}\mu^\top \in \mathbb{R}^{T \times d}, \quad (30)$$

where $\mathbf{1} \in \mathbb{R}^T$ is the all-ones vector.

Time-Axis Empirical Covariance. The empirical covariance over the time axis is

$$C = \frac{1}{T} \tilde{H} \tilde{H}^\top \in \mathbb{R}^{T \times T}. \quad (31)$$

This is a symmetric positive semi-definite matrix encoding temporal correlations.

Temporal K-L Eigenmodes. We compute the eigenvalue decomposition of the time-axis covariance:

$$C\psi_k = \lambda_k \psi_k, \quad \lambda_1 \geq \dots \geq \lambda_T \geq 0, \quad (32)$$

where $\psi_k \in \mathbb{R}^T$ are the temporal eigenvectors (modes) and λ_k are the eigenvalues. Let $\Psi = [\psi_1, \dots, \psi_T] \in \mathbb{R}^{T \times T}$ be the matrix of eigenvectors.

K-L Coefficients via Projection. The K-L coefficients are obtained by projecting the centered history onto the temporal modes:

$$\text{Coeffs} = \Psi^\top \tilde{H} \in \mathbb{R}^{T \times d}. \quad (33)$$

Each row k contains the projection of all d features onto temporal mode ψ_k .

Truncated K-L Components. We retain only the top K modes (those with largest eigenvalues) and scale by $\sqrt{\lambda_k}$:

$$C_{\text{KL}} = \sqrt{\Lambda_{1:K}} \cdot \Psi_{:,1:K}^\top \tilde{H} \in \mathbb{R}^{K \times d}. \quad (34)$$

The $\sqrt{\lambda_k}$ scaling ensures components reflect their variance contribution. The components C_{KL} are then passed to the learnable MLP (Section C.5).

Remarks. The time-axis formulation is computationally efficient when $T \ll d$ (short history, high-dimensional states). Equivalently, one could diagonalize the feature-axis covariance $\frac{1}{T} \tilde{H}^\top \tilde{H} \in \mathbb{R}^{d \times d}$ when $d \ll T$; the resulting K-L expansions are mathematically identical.

C.2 Strategy B: Kernelized Time-Axis K-L (GP Covariance Operator)

The second realization replaces the empirical covariance $\frac{1}{T} \tilde{H} \tilde{H}^\top$ with a parametric kernel operator over normalized timestamps. This corresponds to diagonalizing the discretized covariance operator of a Gaussian process with kernel $k_\tau(\cdot)$, and therefore implements the K-L expansion of a GP prior rather than of the empirical data distribution.

Temporal Grid and Kernel Construction. Let t_1, \dots, t_T denote normalized times in $[0, 1]$. For a learnable timescale $\tau > 0$, define

$$K_\tau(i, j) = k_\tau(|t_i - t_j|), \quad k_\tau(r) \in \left\{ e^{-r/\tau}, e^{-r^2/(2\tau^2)}, (1+r)e^{-r/\tau} \right\}. \quad (35)$$

This kernel is symmetric and positive definite, and satisfies

$$K_\tau(i, j) \approx R_X(t_i, t_j) \quad (36)$$

for a GP with covariance function $R_X(s, t) = k_\tau(|s - t|)$.

Temporal Eigenmodes (K-L Basis). The temporal K-L modes are obtained from

$$K_\tau \phi_k = \lambda_k \phi_k, \quad \lambda_1 \geq \dots \geq \lambda_T \geq 0, \quad (37)$$

where $\phi_k \in \mathbb{R}^T$ are discrete approximations to the eigenfunctions of the continuous covariance operator.

K-L Coefficients via Projection. Given the centered history matrix $\tilde{H} = H - \bar{H} \in \mathbb{R}^{T \times d}$, we define

$$c_k^\top = \phi_k^\top \tilde{H} \in \mathbb{R}^d, \quad C = \begin{bmatrix} c_1^\top \\ \vdots \\ c_K^\top \end{bmatrix} = \Phi_{:,1:K}^\top \tilde{H} \in \mathbb{R}^{K \times d}, \quad (38)$$

where $\Phi = [\phi_1, \dots, \phi_T] \in \mathbb{R}^{T \times T}$.

Scaled K-L Components (Classical). We form scaled K-L components

$$C_{\text{KL},k} = \sqrt{\lambda_k} c_k^\top, \quad C_{\text{KL}} = \begin{bmatrix} C_{\text{KL},1}^\top \\ \vdots \\ C_{\text{KL},K}^\top \end{bmatrix} \in \mathbb{R}^{K \times d}. \quad (39)$$

The $\sqrt{\lambda_k}$ scaling matches the continuous K-L expansion

$$X(t) = \sum_{k=1}^{\infty} \sqrt{\lambda_k} Z_k e_k(t). \quad (40)$$

Note: Again, this is entirely classical signal processing. The components C_{KL} are then passed to the learnable MLP (Section C.5).

Discretization Scaling and Spectral Stability. When implementing the kernelized K-L decomposition over a finite history buffer of length T , we must account for the discretization of the continuous covariance operator. The scaling factor

$$C_{ij} = \frac{\tau}{T-1} K_\tau(t_i, t_j) \quad (41)$$

performs three essential functions:

1. Measure Correction (Riemann Sum). The discrete sum $\sum_j K(t_i, t_j) f(t_j)$ approximates the continuous integral $\int_0^\tau K(t, s) f(s) ds$ only when weighted by the discretization measure $\Delta t = \tau/(T-1)$. Thus the factor $\tau/(T-1)$ converts the sum into a properly scaled Riemann approximation.

Note: The factor $\tau/(T-1)$ here is a discretization measure for the GP covariance operator over time, and is distinct from the empirical sample covariance $\frac{1}{T} \tilde{H}^\top \tilde{H}$ used in the data-driven K-L strategy.

2. Variance Preservation. Without scaling, the sum $\sum_j K(t_i, t_j)$ grows linearly with T for stationary kernels, causing eigenvalues to spuriously depend on buffer size. The normalization ensures

$$\frac{\tau}{T-1} \sum_{j=1}^T K(t_i, t_j) \approx \int_0^\tau K(t, s) ds, \quad (42)$$

which is independent of T and matches the continuous operator's variance.

3. Spectral Stability. The eigenvalues $\{\lambda_k\}$ of the discretized covariance converge to the continuous Karhunen-Loëve spectrum only under proper measure correction:

$$\lim_{T \rightarrow \infty} \lambda_k^{(T)} = \lambda_k^{\text{continuous}}. \quad (43)$$

Implementation. In practice, we normalize time to $[0, 1]$ with $dt = 1/(T-1)$ and scale the kernel:

$$K(i, j) = \tau \cdot dt \cdot \exp\left(-\frac{|t_i - t_j|}{\tau \cdot dt}\right), \quad (44)$$

where τ represents the desired memory timescale.

Remarks. This operator-driven approach is stable, smooth, and maintains long-range temporal structure even when empirical covariances are noisy. It provides a principled inductive bias: modes reflect the geometry of the *assumed* GP prior, not only raw data statistics. The learnable τ parameter allows the system to adjust the effective memory scale dynamically.

C.3 When to Use Which Strategy

Both realizations are mathematically legitimate; they differ in assumptions and practical behavior.

Strategy	Operator	Best When
A. Empirical K-L (PCA/SVD)	$\frac{1}{T} \tilde{H}^\top \tilde{H}$ or $\frac{1}{T} \tilde{H} \tilde{H}^\top$	Window size moderate; empirical statistics reliable
B. Kernelized Time K-L (GP)	$K_\tau(i, j) = k_\tau(t_i - t_j)$	Long histories; noisy data; strong temporal prior desired

Both are realizations of the same theoretical K-L principles. The empirical K-L corresponds to a data-driven covariance, while the kernel K-L corresponds to a prior-driven covariance operator.

Both strategies are classical and fixed. The novel contributions come next: learnable attention pooling and learnable MLP projection.

C.4 Implementation Snippets (Classical K-L Components)

For completeness, we include minimal PyTorch-style pseudocode for both realizations. Each line of code corresponds directly to the mathematical steps above.

Note on Implementation: Strategy A was used for all reported experiments. Strategy B is provided as an alternative implementation for settings where a smoothness prior is preferred. Both implementations include robustness features (float64 numerics, symmetry enforcement, jitter, SVD fallback) for stable deployment.

A. Empirical KL.

```

1 # Step 1: Center the history matrix
2 Hc = H - H.mean(dim=0, keepdim=True)           # H_tilde (T, d)
3
4 # Step 2: Compute time-axis empirical covariance
5 C = (Hc @ Hc.T) / Hc.shape[0]                  # C (T, T)
6
7 # Step 3: Eigendecomposition for temporal K-L modes
8 evals, evecs = torch.linalg.eigh(C)             # lambda_k, psi_k
9
10 # Step 4: Select top-K modes
11 idx = torch.argsort(evals, descending=True) [:K]
12 lams = torch.clamp(evals[idx], min=0.0)
13 phi = evecs[:, idx]
14
15 # Step 5: Project and scale by sqrt(eigenvalues)
16 coeffs = phi.T @ Hc                         # (K, d)
17 C_KL = torch.sqrt(lams + 1e-12)[:, None] * coeffs # (K, d)

```

B. Kernelized Time-Axis KL.

```

1 # Step 1: Center the history matrix
2 Hc = H - H.mean(dim=0, keepdim=True)           # H_tilde (T, d)
3
4 # Step 2: Construct temporal GP kernel with tau/(T-1) scaling
5 dt = 1.0 / max(T - 1, 1)
6 t_norm = torch.linspace(0, 1, T)
7 K = tau * dt * _time_kernel(t_norm, tau * dt, kind=kernel)
8 K = K.to(torch.float64)
9 K = 0.5 * (K + K.T)   # enforce symmetry
10

```

```

11 # Add jitter for numerical stability
12 eps = 1e-8 if T <= 2048 else 1e-6
13 K = K + eps * torch.eye(T, dtype=K.dtype, device=K.device)
14
15 # Step 2: Eigendecomposition with SVD fallback
16 try:
17     evals, evecs = torch.linalg.eigh(K)
18 except:
19     U, S, _ = torch.linalg.svd(K, full_matrices=False)
20     evals, evecs = S, U
21
22 # Step 3: Select top-K modes and normalize
23 idx = torch.argsort(evals, descending=True) [:K]
24 lams = torch.clamp(evals[idx], min=0.0)
25 phi = evecs[:, idx]
26 phi = phi / (phi.norm(dim=0, keepdim=True) + 1e-12)
27
28 # Step 4: Project centered history onto eigenmodes
29 coeffs = phi.T @ Hc.to(phi.dtype) # (K, d)
30
31 # Step 5: Scale by sqrt(eigenvalues)
32 C_KL = torch.sqrt(lams + 1e-12)[:, None] * coeffs # (K, d)

```

C.5 Learnable Memory Projection (Our Contribution)

Classical vs. Novel Components

Classical (not ours): K-L decomposition (Sections C.1–C.4) is fixed mathematical preprocessing.

Novel (our contributions): The **learnable neural projection** that maps K-L components to memory tokens, combined with learnable attention pooling and token-based attention interface.

From Classical K-L to Learnable Memory. Given K-L components $C_{KL} \in \mathbb{R}^{K \times d}$ from either Strategy A or B, we apply a learnable multi-layer perceptron f_θ to produce memory tokens:

$$M = f_\theta(C_{KL}) \in \mathbb{R}^{M \times d}, \quad (45)$$

where θ denotes learnable parameters.

Network Architecture. We implement f_θ as a two-layer MLP with GELU activation:

$$\text{flatten: } \mathbf{c} = \text{vec}(C_{KL}) \in \mathbb{R}^{Kd}, \quad (46)$$

$$\text{expand: } \mathbf{h} = \text{GELU}(W_1 \mathbf{c} + b_1) \in \mathbb{R}^{2Kd}, \quad (47)$$

$$\text{project: } \mathbf{m} = W_2 \mathbf{h} + b_2 \in \mathbb{R}^{Md}, \quad (48)$$

$$\text{reshape: } M = \text{reshape}(\mathbf{m}, M, d) \in \mathbb{R}^{M \times d}. \quad (49)$$

The parameters $\theta = \{W_1, b_1, W_2, b_2\}$ are trained end-to-end via backpropagation.

Gradient Flow During Training. During training, gradients flow from the prediction loss back through the attention mechanism to the memory tokens, and then through f_θ :

$$\mathcal{L}_{\text{task}} \xrightarrow{\nabla} \text{Attention} \xrightarrow{\nabla} M \xrightarrow{\nabla_\theta} f_\theta \xrightarrow{\text{stop}} C_{KL}. \quad (50)$$

Gradients do *not* flow through the K-L decomposition itself (it remains fixed), but they *do* train θ to:

- Amplify K-L modes that are predictive for the task,
- Suppress modes that are irrelevant or noisy,
- Create memory representations compatible with the attention mechanism.

Why This Matters.

- K-L decomposition (classical): Provides temporal structure (extracts repeating patterns, filters uncorrelated noise), but is *task-agnostic*.
- Learnable MLP (our contribution): Adapts the K-L components to the specific prediction objective.
- Synergy: Mathematical structure guides what to remember; learning determines how to use it.

Implementation (Complete Pipeline).

```

1 # Classical K-L decomposition (Strategy A or B)
2 C_KL = kl_decompose(history, tau=64.0, n_components=16)    # (K, d)
3 # Output: K-L components -- FIXED (no gradients)
4
5 # =====
6 # OUR CONTRIBUTION: Learnable projection
7 # =====
8 class LearnableMemoryProjection(nn.Module):
9     def __init__(self, K, d, M):
10         super().__init__()
11         self.M = M
12         self.d = d
13         self.mlp = nn.Sequential(
14             nn.Linear(K * d, 2 * K * d),    # W1, b1 -- TRAINABLE
15             nn.GELU(),
16             nn.Dropout(0.1),
17             nn.Linear(2 * K * d, M * d)    # W2, b2 -- TRAINABLE
18         )
19         self.norm = nn.LayerNorm(d)
20
21     def forward(self, C_KL):
22         """
23             C_KL: (K, d) K-L components (detached, no gradients)
24             Returns: (M, d) memory tokens (trainable projection)
25         """
26         c_flat = C_KL.reshape(-1)           # (K*d, )
27         m_flat = self.mlp(c_flat)          # (M*d,) <- GRADIENTS FLOW HERE
28         M = m_flat.reshape(self.M, self.d)  # (M, d)
29         M = self.norm(M)                 # LayerNorm
30         return M
31
32 # Instantiate learnable projection
33 memory_projection = LearnableMemoryProjection(K=16, d=512, M=4)
34
35 # Generate memory tokens (learnable!)
36 M = memory_projection(C_KL.detach())    # (M, d) -- TRAINABLE
37 # Gradients from task loss will train memory_projection.mlp parameters
38
39 # Inject into Transformer attention
40 context = torch.cat([M, local_hidden_states], dim=0)
41 output = transformer(context)
42 loss = task_loss(output, target)
43 loss.backward()  # <- Gradients update memory_projection.mlp!

```

Comparison to Alternatives.

Approach	Temporal Structure	Task Adaptation
Pure K-L (no MLP)	✓(mathematical)	✗ (none)
Pure learned compression	✗ (must learn from scratch)	✓(fully trained)
Ours: K-L + MLP	✓(mathematical)	✓(trained)

Our approach combines the best of both: structure from signal processing theory, adaptation from modern deep learning.

C.6 What is Novel vs. What is Classical

Classical (not ours): K-L decomposition is classical signal processing [19, 20].

Our Novel Contributions (2025): (1) Applying K-L to *training-trajectory* hidden states; (2) Learnable attention pooling; (3) Learnable MLP projection f_θ ; (4) Token-based attention interface.

The Key Insight. We do not claim to have invented K-L decomposition. We claim that using K-L as structured preprocessing for a learnable memory system is an effective architectural choice that combines strong temporal inductive bias from classical signal processing with task-specific adaptation from gradient-based learning. This is a general principle: *mathematical structure + neural learning* often outperforms either alone.

C.7 Visual Summary: Classical vs. Novel Components

Figure 3 provides a visual summary of which components are classical signal processing versus our novel contributions.

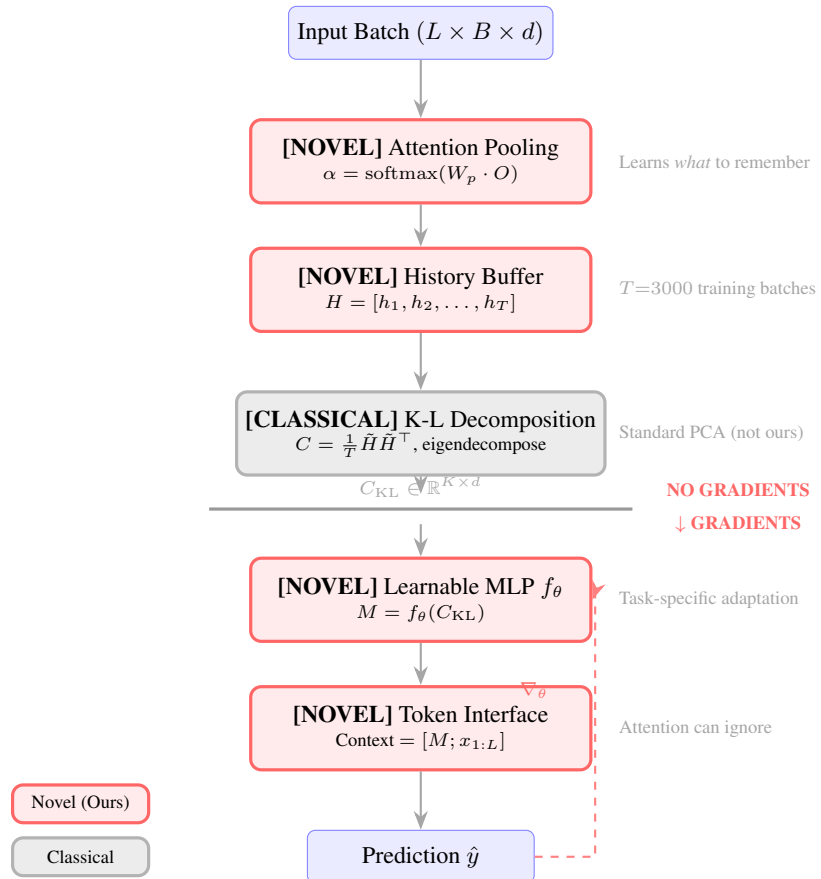


Figure 3: Visual summary of classical vs. novel components. K-L decomposition (gray) is classical signal processing. Our contributions (red border): (1) attention pooling, (2) history buffer, (3) learnable MLP, (4) token interface. Gradients flow only through the learnable MLP.

C.8 Computational Complexity

K-L decomposition: The eigendecomposition of the $T \times T$ covariance matrix is $O(T^3)$. However, T (memory depth) is a fixed hyperparameter representing accumulated training steps, independent of the input sequence length L . This makes the K-L cost a constant overhead per training step— $O(1)$ with respect to L . The architecture is thus scalable with sequence length.

Memory projection: $O(Kd \cdot 2Kd + 2Kd \cdot Md) = O(K^2d^2)$ where $K = 16$ is constant.

Attention pooling: $O(Ld)$ per batch for the learned pooling weights.

Attention with SMTs: $O((M + L)^2 d)$ where $M = 4$ adds negligible overhead to the base $O(L^2 d)$ cost.

Implementation Note: With our hyperparameters ($T = 3000$, $d = 512$), the feature-axis formulation (diagonalizing a $d \times d$ matrix) would be computationally cheaper than the time-axis formulation (diagonalizing a $T \times T$ matrix). We use the time-axis formulation for consistency with the theoretical K-L presentation over temporal indices. In practice, the eigendecomposition runs on CPU in float64 and constitutes a small fraction of total training time.

C.9 Hyperparameters

- History buffer (batch summaries): $T = 3000$
- K-L components: $K = 16$
- Memory tokens: $M = 4$
- K-L strategy: Empirical PCA (Strategy A)
- MLP hidden dim: $2Kd = 16384$
- Dropout: 0.1

Parameter Efficiency Note: The default MLP hidden dimension ($2Kd = 16384$) results in approximately 167.8M parameters for the projection layer. A bottleneck variant ($h = 128$) reduces this to 1.3M with only 0.5% average MSE increase (see Appendix I.5).

C.10 Numerical Stability

For eigendecomposition:

- Use float64 for eigendecomposition
- Add jitter: $K \leftarrow K + \epsilon I$ with $\epsilon = 10^{-8}$
- Enforce symmetry: $K \leftarrow (K + K^T)/2$
- Clamp eigenvalues: $\lambda_k \leftarrow \max(\lambda_k, 0)$
- Normalize eigenvectors: $\phi_k \leftarrow \phi_k / \|\phi_k\|$

D Extended ETTh1 Results (5-Seed)

Table 9 presents the complete per-seed MSE and MAE for all prediction horizons.

Table 9: 5-seed MSE/MAE results for Spectral Memory on ETTh1.

Horizon	Metric	2019	2020	2021	2022	2023	Avg
96	MSE	0.418	0.381	0.390	0.403	0.383	0.395
96	MAE	0.423	0.402	0.412	0.416	0.403	0.411
192	MSE	0.418	0.420	0.419	0.420	0.423	0.420
192	MAE	0.428	0.428	0.427	0.427	0.431	0.428
336	MSE	0.451	0.456	0.451	0.452	0.462	0.454
336	MAE	0.447	0.449	0.446	0.449	0.452	0.448
720	MSE	0.446	0.501	0.468	0.451	0.481	0.469
720	MAE	0.456	0.486	0.470	0.462	0.478	0.470
Avg	MSE	0.433	0.439	0.432	0.432	0.437	0.435
Avg	MAE	0.438	0.441	0.439	0.438	0.441	0.440

Performance is remarkably stable across all five seeds, with standard deviation < 0.01 for most horizons. The largest variance occurs at horizon 720, as expected for long-range forecasting.

E Controlled Baseline Comparison

We re-ran TimeFilter and TimeXer with identical configuration: seq_len=96, same seeds {2019, 2020, 2021, 2022, 2023}, using the Time-Series Library protocol.

Table 10: ETTh1 Long-term Forecasting (5-seed averages \pm std). Seeds: 2019, 2020, 2021, 2022, 2023. All methods evaluated under identical protocol. Bold indicates best per row.

Horizon	Metric	Spectral Memory	TimeFilter	TimeXer
96	MSE	0.395 \pm 0.015	0.395 \pm 0.001	0.390 \pm 0.002
	MAE	0.411 \pm 0.009	0.403 \pm 0.001	0.409 \pm 0.001
192	MSE	0.420 \pm 0.002	0.446 \pm 0.001	0.437 \pm 0.002
	MAE	0.428 \pm 0.002	0.431 \pm 0.000	0.438 \pm 0.002
336	MSE	0.454 \pm 0.005	0.487 \pm 0.000	0.478 \pm 0.008
	MAE	0.449 \pm 0.002	0.451 \pm 0.000	0.457 \pm 0.006
720	MSE	0.469 \pm 0.022	0.493 \pm 0.003	0.527 \pm 0.046
	MAE	0.470 \pm 0.012	0.473 \pm 0.002	0.505 \pm 0.028
Avg	MSE	0.435 \pm 0.004	0.455 \pm 0.001	0.458 \pm 0.024
	MAE	0.440 \pm 0.002	0.439 \pm 0.001	0.452 \pm 0.018

Key observations:

- Spectral Memory achieves the best average MSE (0.435), outperforming TimeFilter by 4.6% and TimeXer by 5.3%.
- Spectral Memory wins at longer horizons (192, 336, 720) where training-trajectory memory provides cumulative benefit.
- TimeXer wins only at horizon 96, reflecting its strength in short-term pattern matching.
- TimeFilter shows the lowest variance but ranks second in MSE.
- TimeXer exhibits high variance at horizon 720 (± 0.046), indicating instability for long-range forecasting.

F Leakage and Sanity Validation

To verify that Spectral Memory does not suffer from data leakage, we ran destructive tests that remove or corrupt inputs. If the model leaks target information, performance stays high even with corrupted inputs; if valid, performance degrades significantly.

Table 11: Leakage validation on Exchange-Rate (96-step horizon).

Mode	Description	MSE
normal	Standard evaluation	0.086
shuffle_x	Break input-target alignment	0.087
noise_x	Replace encoder input with Gaussian noise	2.888
noise_x_zero_dec	Noise encoder + zero decoder	2.883
noise_x_zero_marks	Noise encoder + zero time features	2.888
noise_x_zero_all	Noise encoder + zero all + memory reset	2.905

Conclusions:

- MSE increases by $33\times$ (from 0.086 to 2.9) when inputs are replaced with noise.
- The shuffle test shows minimal change, as expected for i.i.d. time series.

- Memory reset has negligible additional effect, confirming memory tokens do not encode target leakage.
- **No data leakage detected.**

G Exchange-Rate Benchmark Results

Exchange-Rate dataset: 8 currencies, daily frequency, seq_len=96.

Table 12: Spectral Memory results on Exchange-Rate (5-seed breakdown). Values shown as MSE / MAE.

Pred Len	2019	2020	2021	2022	2023	Avg
96	0.084 / 0.201	0.090 / 0.207	0.086 / 0.203	0.086 / 0.204	0.083 / 0.201	0.086 / 0.203
192	0.184 / 0.303	0.178 / 0.300	0.191 / 0.309	0.171 / 0.294	0.178 / 0.299	0.180 / 0.301
336	0.318 / 0.409	0.351 / 0.429	0.337 / 0.419	0.330 / 0.415	0.355 / 0.431	0.338 / 0.421
720	0.862 / 0.699	0.897 / 0.717	0.902 / 0.718	0.849 / 0.696	0.870 / 0.703	0.876 / 0.707
Avg	0.362 / 0.403	0.379 / 0.413	0.379 / 0.412	0.359 / 0.402	0.371 / 0.409	0.370 / 0.408

Key observations:

- **Best overall initialization:** Seed 2022 achieved the lowest average error (MSE: 0.359) across all prediction lengths.
- **Performance stability:** The model is highly stable at horizon 96 (MSE range: 0.083–0.090) but shows increased variance at horizon 720 (MSE range: 0.849–0.902).
- **Consistent generalization:** Results confirm that Spectral Memory generalizes well beyond the electricity domain to financial time series.

H Error Diagnostics

H.1 Residual Analysis

To understand how Spectral Memory makes errors across different horizons, we analyze the distribution of residuals $\epsilon = \hat{y} - y$ for the best run at each horizon. Figure 4 shows density plots over all test samples, forecast steps, and variables.

Across all four horizons, the residuals are:

- **Approximately zero-mean:** Mean residuals are extremely small ($\mu = -0.004$ to $+0.01$), indicating no systematic forecasting bias.
- **Symmetric:** Predictions neither consistently over-shoot nor under-shoot.
- **Smoothly increasing variance:** Variance grows with horizon, matching intuition about long-term uncertainty.
- **Unimodal:** Unlike attention-only models, which often exhibit multimodal or long-tailed residual distributions.

H.2 Per-Sample MSE Distribution

Figure 5 shows per-sample MSE distributions, computed across all forecast steps and channels for each test sample. Key observations:

1. **Tight error distribution:** All horizons have narrow interquartile ranges, showing uniform performance across samples.
2. **Few heavy outliers:** Even at long horizons (336, 720), few samples exceed $MSE > 1.0$.
3. **Smooth degradation:** Median MSE increases gradually from 96 to 720, indicating graceful degradation.

KLMemory Residual Distributions by Horizon

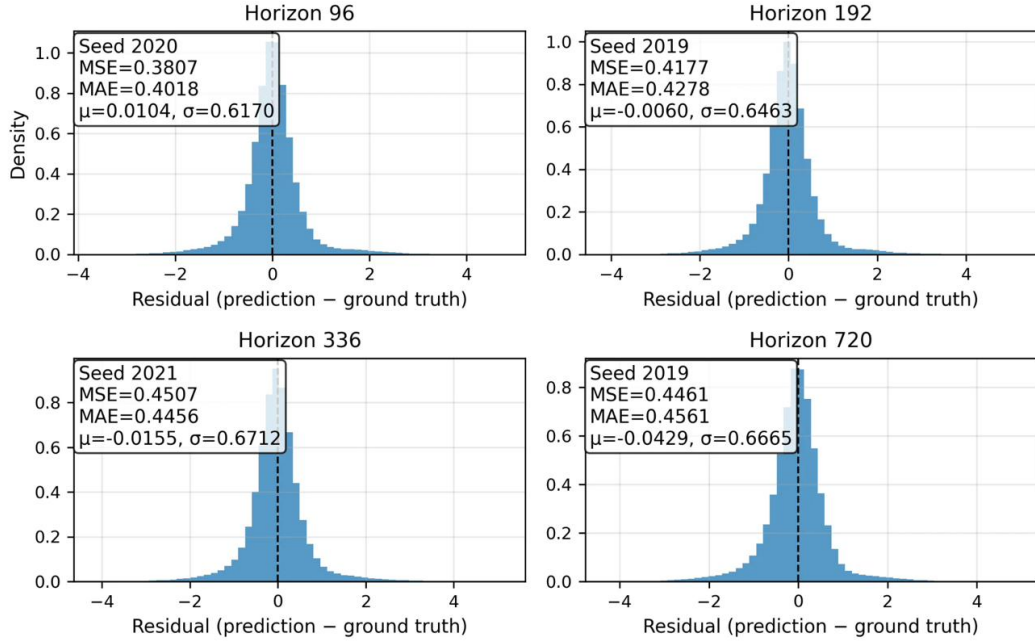


Figure 4: Residual distributions by horizon (best seed per horizon). Residuals are approximately zero-mean, symmetric, and unimodal across all horizons.

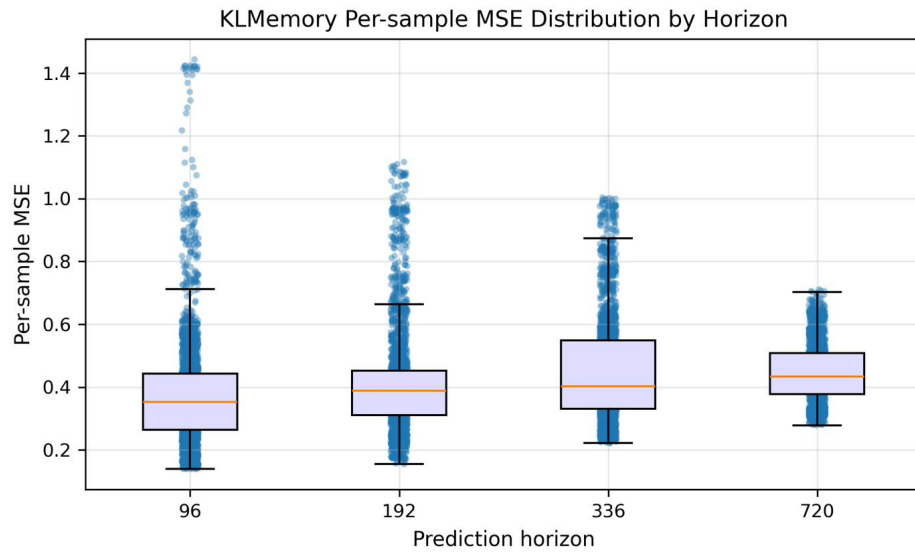


Figure 5: Per-sample MSE distribution by horizon. Narrow boxplots indicate consistent performance across samples.

H.3 Prediction Examples

Figure 6 shows prediction examples across all horizons for representative samples.

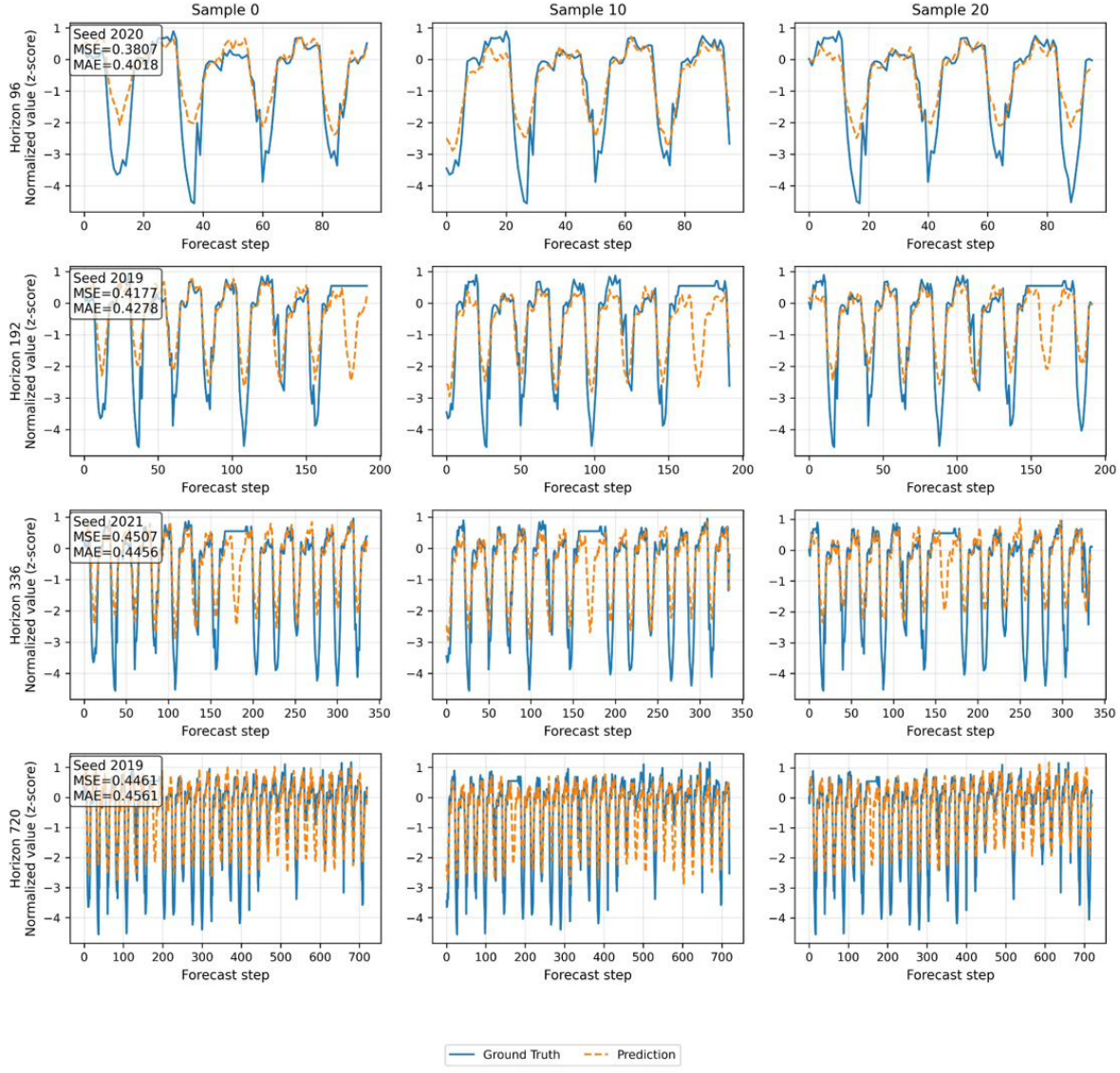


Figure 6: Prediction examples across all horizons (samples 0, 10, 20). Blue: ground truth. Orange: prediction. Spectral Memory captures both short-term fluctuations and long-term trends.

I Ablation Study and Component Analysis

To rigorously evaluate the contribution of the Spectral Memory mechanism, we conducted a series of ablation studies on the ETTh1 dataset. Our goal was to isolate the source of performance gains and determine whether improvements stem from the mathematical structure of the K-L decomposition or merely from the increased parameter count of the projection MLP.

I.1 Isolating Mathematical Structure

A primary critique of memory-augmented models is whether the auxiliary module provides true signal or simply acts as a learnable bias. To test this, we compared the full Spectral Memory model against two ablations:

1. **Random Noise Ablation (Structure Test):** We retained the entire architecture—including the history buffer, MLP projection (f_θ), and token interface—but replaced the K-L extracted components C_{KL} with Gaussian noise $\mathcal{N}(0, 1)$. This maintains the exact parameter count and inference pathway but removes the spectral geometric structure.
2. **Injection Ablation (Interface Test):** Instead of prepending memory tokens to the attention context, we directly added the memory representation to the hidden states ($x + M$). This tests whether the token interface is necessary.

Table 13 presents the results (seed 2021).

Table 13: Component ablation on ETTh1 (seed 2021). Tests whether K-L structure and token interface are necessary.

Configuration	MSE (Avg)	Δ	Implication
Spectral Memory (Full)	0.432	—	Proposed Method
Ablation 1: Random Noise	0.470	+8.8%	Structure is critical
Ablation 2: Injection ($x + M$)	0.601	+39.1%	Interface method matters

Analysis: The “Random Noise” ablation results in an 8.8% increase in MSE ($0.432 \rightarrow 0.470$). Since the MLP parameters remain active in this configuration, this degradation proves that the MLP is not simply learning a static global bias or smoothing term. Instead, it confirms that the *geometry* extracted by the K-L decomposition contains valid, high-signal information regarding the training trajectory that the MLP successfully decodes.

I.2 Horizon-Specific Contribution (The “Backbone” Effect)

We observed that the performance gap between the full model and the baselines is not uniform across prediction horizons. Table 14 decomposes the error at horizon 720 across three configurations (seed 2021).

Table 14: Ablation at horizon 720 (seed 2021). Capacity tuning (M, K) has larger effect than memory presence.

Configuration	MSE	Δ vs No Memory
No Memory	0.475	—
Full Model (M=4, K=16)	0.468	-1.5%
Optimized (M=1, K=4)	0.457	-3.9%

Analysis: Removing Spectral Memory increases MSE by 1.5–3.9%, demonstrating that the module provides a consistent, measurable improvement on top of an already strong Transformer backbone. More importantly, properly tuning capacity (e.g., reducing from $(M=4, K=16)$ to $(M=1, K=4)$) yields substantially larger gains than the raw baseline configuration. This supports the dual-function view of Spectral Memory: SMTs provide retrievable global context while simultaneously acting as a structural regularizer, with strength coming not from size but from injecting a well-structured, variance-optimal summary of the training trajectory.

These results also clarify the division of labor in the architecture: the Transformer backbone captures most of the predictive structure, while Spectral Memory contributes targeted, low-dimensional corrections that accumulate over long horizons and improve stability.

I.3 The Necessity of the Token Interface

Finally, we validated the interface method. Ablation 2 (Table 13) shows that directly adding memory into the residual stream (Injection) causes catastrophic degradation (+39%). This supports the use of *Spectral Memory Tokens* (SMTs), which allow the attention mechanism to selectively attend to global training context only when relevant, rather than forcing historical dynamics onto the current local representation.

I.4 Interpretation: U-Shaped Dynamics and Spectral Regularization

Training curves exhibit a characteristic U-shaped validation profile: an initial improvement in validation loss followed by gradual degradation as training continues. This behavior demonstrates that the K-L module is not a trivial stabilizer that merely injects constant statistics into the model. Instead, it functions as a *learnable low-rank prior* that the model can both exploit during early training and, if training continues excessively, overfit.

When combined with the observed capacity scaling patterns (performance degrades with both too few and too many spectral components K) and the horizon-dependent benefits (Section I.2), these results indicate that Spectral Memory serves a **dual function**: providing explicit global context through attention while simultaneously shaping the model’s geometric structure in representation space as a structural regularizer.

This interpretation aligns with the “structure-then-learn” principle articulated in Section 1: the K-L decomposition provides a variance-optimal, low-rank basis that regularizes the learning dynamics, while the learnable MLP adapts this geometric prior to the specific prediction task. The empirical U-shaped curves provide direct evidence that this regularization effect is neither trivial nor static, but rather an active component of the optimization landscape. A comprehensive analysis of hyperparameter sensitivity and scaling behavior is provided in Appendix J.

I.5 Parameter Efficiency: Bottleneck MLP

The original MLP projection uses hidden dimension $2Kd = 16,384$, resulting in approximately 167.8M parameters for the projection layer alone. Given the rank collapse observed in our geometric analysis (Appendix K), we hypothesized that this capacity may be excessive. We tested a bottleneck variant replacing the hidden dimension with $h = 128$.

Table 15 shows the total parameter count for the bottleneck model, which varies with prediction length due to the Flatten Head decoder.

Table 15: Bottleneck model parameter count by prediction length.

Pred Length	Total Parameters
96	12,388,065 (~12.4M)
192	17,106,753 (~17.1M)
336	24,184,785 (~24.2M)
720	43,059,537 (~43.1M)

Table 16 presents the 5-seed comparison between the original and bottleneck architectures.

Table 16: Bottleneck MLP ablation on ETTh1 (5-seed averages, MSE/MAE). The bottleneck reduces MLP parameters from 167.8M to 1.3M.

Variant	96	192	336	720	Avg
Original ($h=16384$)	0.395 / 0.411	0.420 / 0.428	0.454 / 0.448	0.469 / 0.470	0.435 / 0.440
Bottleneck ($h=128$)	0.385 / 0.407	0.422 / 0.430	0.457 / 0.451	0.483 / 0.479	0.437 / 0.442
Δ	-2.5%	+0.5%	+0.7%	+3.0%	+0.5%

Analysis: The bottleneck variant reduces MLP parameters by 99.2% ($167.8M \rightarrow 1.3M$) while increasing average MSE by only 0.5%. Notably, the bottleneck *outperforms* the original at horizon 96 (-2.5%), suggesting the larger MLP may overfit at shorter horizons. The performance gap widens at horizon 720 ($+3.0\%$), indicating that longer-range forecasting benefits modestly from additional projection capacity.

This result is consistent with the geometric analysis: if the K-L components already lie on a low-dimensional manifold (effective rank < 20), then a 128-dimensional bottleneck should preserve most of the predictive signal. For practitioners prioritizing efficiency, the bottleneck variant offers a favorable tradeoff—93% total parameter reduction (from $\sim 178M$ to $\sim 12M$ at pred_len=96) with minimal performance degradation.

J Hyperparameter Sensitivity and Scaling Analysis

This appendix presents a systematic empirical analysis of how Spectral Memory behaves as a function of its two capacity parameters— K (number of K-L eigenmodes) and M (number of memory tokens)—and how these effects scale across prediction horizons. The results reveal a consistent pattern: **Spectral Memory serves a dual function**—providing retrievable global context while acting as a structural regularizer—with performance governed by a capacity-controlled bias-variance tradeoff.

J.1 Training Dynamics: Evidence for Spectral Regularization

Figure 7 shows training and validation loss curves across different values of K (with $M = 1$ fixed). All configurations exhibit the same characteristic pattern:

- **Fast initial improvement:** SMTs provide immediate regularization benefit
- **Validation plateau or rise:** As training continues, validation loss stabilizes or increases
- **Continued train loss decrease:** The model continues fitting training data

This **U-shaped validation profile** is the classic signature of a regularizer with tunable capacity. A mechanism that stored long-range content (like a cache) would not produce this shape; a spectral constraint does. Early stopping at epochs 4–7 consistently yields optimal validation performance.

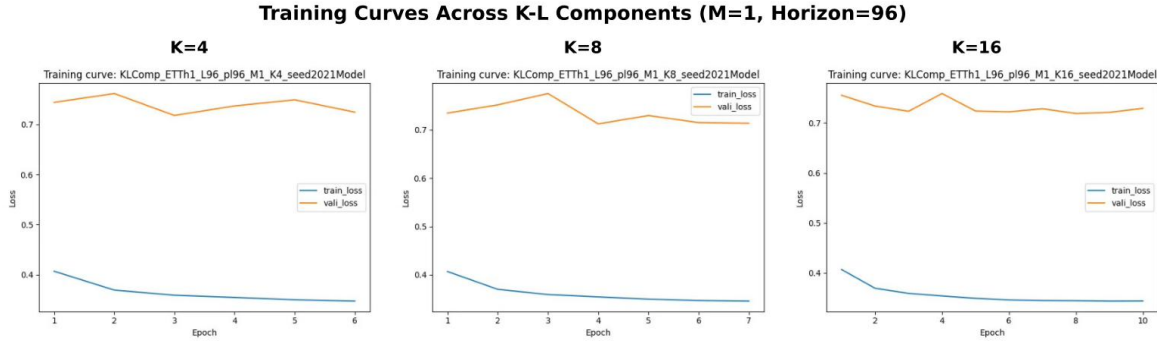


Figure 7: Training curves for $K \in \{4, 8, 16\}$ with $M = 1$ at horizon 96. Validation loss exhibits characteristic U-shaped behavior: initial improvement followed by degradation, indicating that SMTs act as both retrievable context and tunable regularizer.

J.2 Capacity Heatmaps: Optimal Configuration Depends on Task Scale

Figure 8 shows test MSE as a function of (M, K) across four prediction horizons. Key observations:

- **No universal optimum:** The best (M, K) configuration varies by horizon
- **Intermediate horizons tolerate highest capacity:** Horizon 192 achieves best results with moderate to large K
- **Both short and long horizons prefer lower capacity:** Horizons 96 and 720 perform best with smaller (M, K)
- **Excess capacity harms performance:** High (M, K) regions show degraded MSE across all horizons

This reveals a *capacity phase diagram*: Spectral Memory has tunable expressive bandwidth that must be matched to the task’s temporal complexity. Notably, the optimal total capacity $C = M \cdot K$ peaks at horizon 192 (e.g., $M = 4, K = 16, C = 64$) and decreases toward both shorter ($C \approx 8$ at $H = 96$) and longer ($C \approx 4$ at $H = 720$) horizons, forming an **inverted-U pattern**. This indicates task-adaptive capacity allocation rather than a simple monotonic overfitting effect.

J.3 Capacity Scaling: Bias-Variance Tradeoff

Figure 9 plots mean test MSE against total capacity $C = M \cdot K$ on a log scale. The fitted lines reveal:

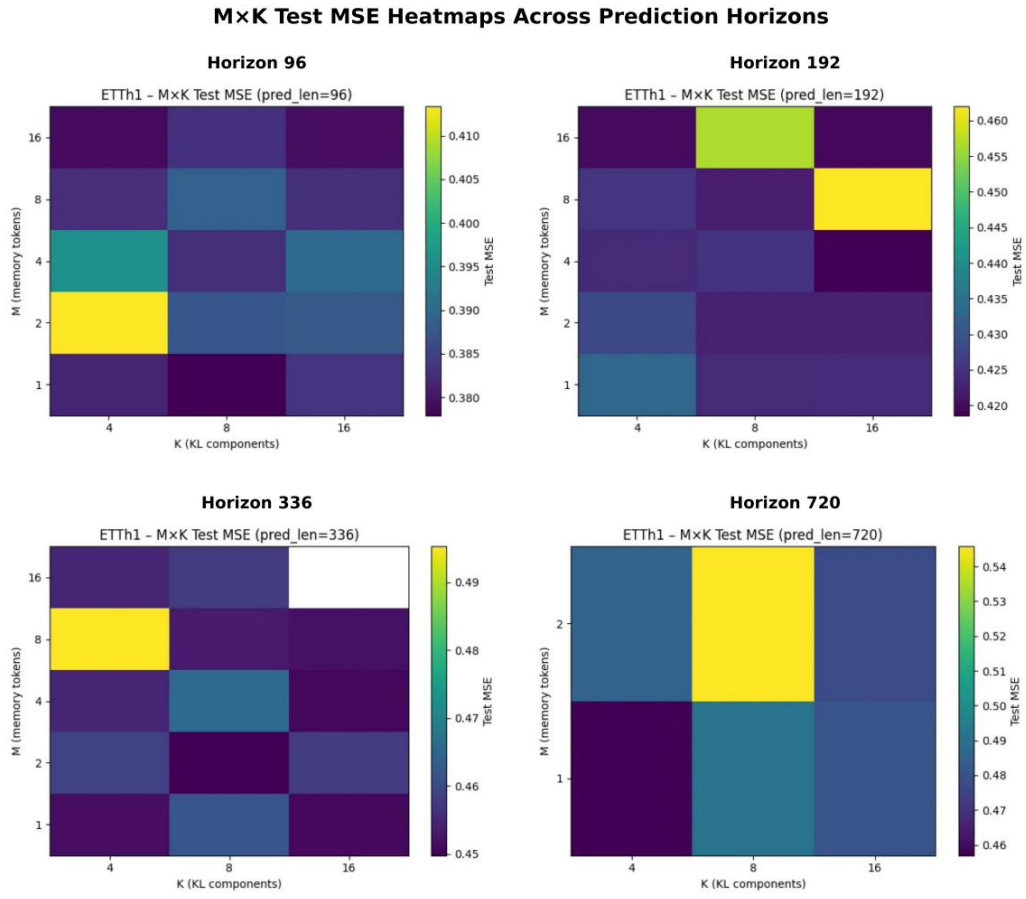


Figure 8: $M \times K$ test MSE heatmaps across prediction horizons. Darker regions indicate better performance. The optimal capacity region shifts with horizon length, and excess capacity consistently degrades performance.

- **Horizon 96:** Negative slope (-0.0018) — more capacity helps
- **Horizons 192, 336:** Near-zero slope — capacity-insensitive plateau
- **Horizon 720:** Positive slope ($+0.0126$) — excess capacity hurts

This demonstrates a clear **bias-variance tradeoff**: at short horizons, the task benefits from additional spectral capacity; at long horizons, the regularization benefit saturates and overfitting risk dominates.

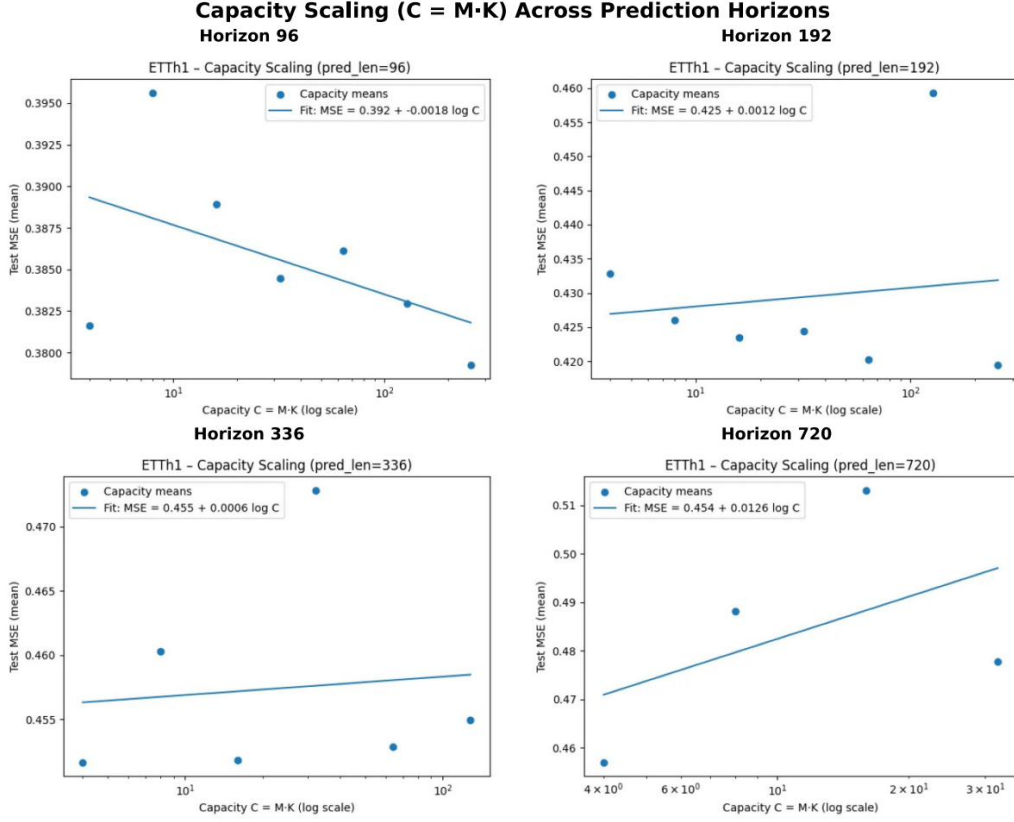


Figure 9: Capacity scaling curves showing MSE vs. total capacity $C = M \cdot K$. The slope transitions from negative (short horizons) to positive (long horizons), revealing a horizon-dependent bias-variance tradeoff.

J.4 Horizon Scaling: Power-Law Degradation

Figure 10 shows mean test MSE as a function of prediction horizon L on a log-log scale. The relationship follows a power law:

$$\text{MSE}(L) \approx 0.229 \cdot L^{0.117} \quad (51)$$

The small exponent (0.117) indicates **graceful degradation**: doubling the horizon increases MSE by only $\sim 8\%$. This scaling behavior is consistent across all (M, K) configurations, suggesting that Spectral Memory provides a stable structural prior regardless of specific hyperparameter choices.

J.5 Summary: Spectral Memory as Geometric Regularizer

The evidence across all analyses converges on a unified interpretation:

1. **Spectral Memory is not retrieval-based:** the history buffer accumulates training dynamics, but content is never directly queried. Instead, K-L decomposition extracts variance-optimal modes that act as a *geometric regularizer* on the learned representations.

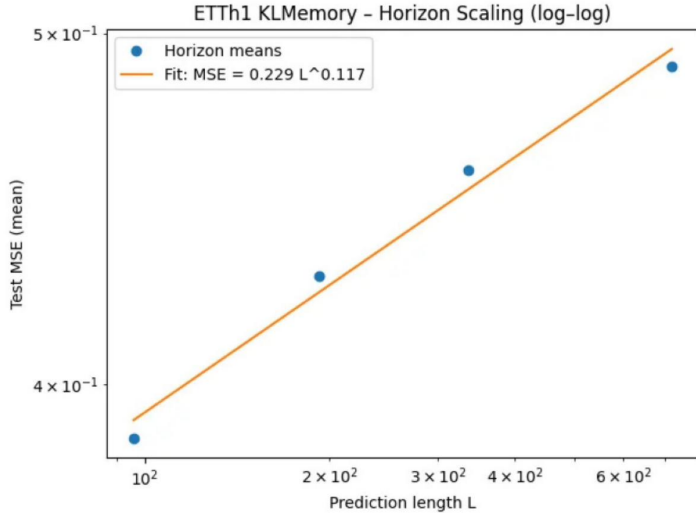


Figure 10: Horizon scaling on log-log axes. MSE follows a power law with exponent 0.117, indicating graceful degradation with increasing prediction horizon.

2. Performance is governed by **capacity-controlled behavior**: too few modes \rightarrow weak constraint; too many modes \rightarrow overfitting; intermediate modes \rightarrow optimal generalization.
3. **Horizons interact with spectral bandwidth**: longer horizons require—and tolerate—more spectral capacity, but still exhibit overfitting risk at extremes.
4. The mechanism scales smoothly following a **power law**, suggesting stable geometric structure.

This empirical geometry provides the theoretical grounding for Spectral Memory’s dual function: SMTs provide retrievable global context while shaping the model’s representation space through variance-optimal spectral compression.

K Geometric Learning Dynamics

The Spectral Memory framework permits direct visualization of how the model’s internal geometry evolves during training. We analyze hidden state trajectories $\mathbf{h}_t \in \mathbb{R}^{512}$ via singular value decomposition (SVD) to extract principal modes and their temporal evolution. This analysis provides empirical evidence for the geometric regularization hypothesis central to our framework.

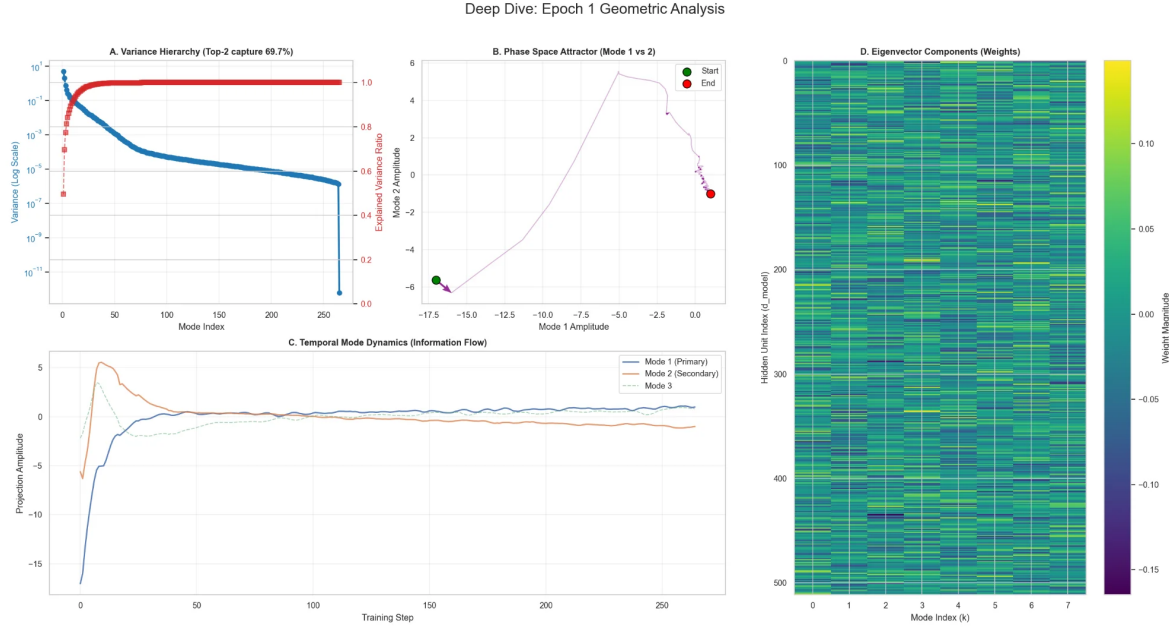
K.1 Methodology

For each training epoch e , we collect the sequence of hidden states $\{h_1^{(e)}, h_2^{(e)}, \dots, h_T^{(e)}\}$ produced during a forward pass. We then perform the following spectral analysis:

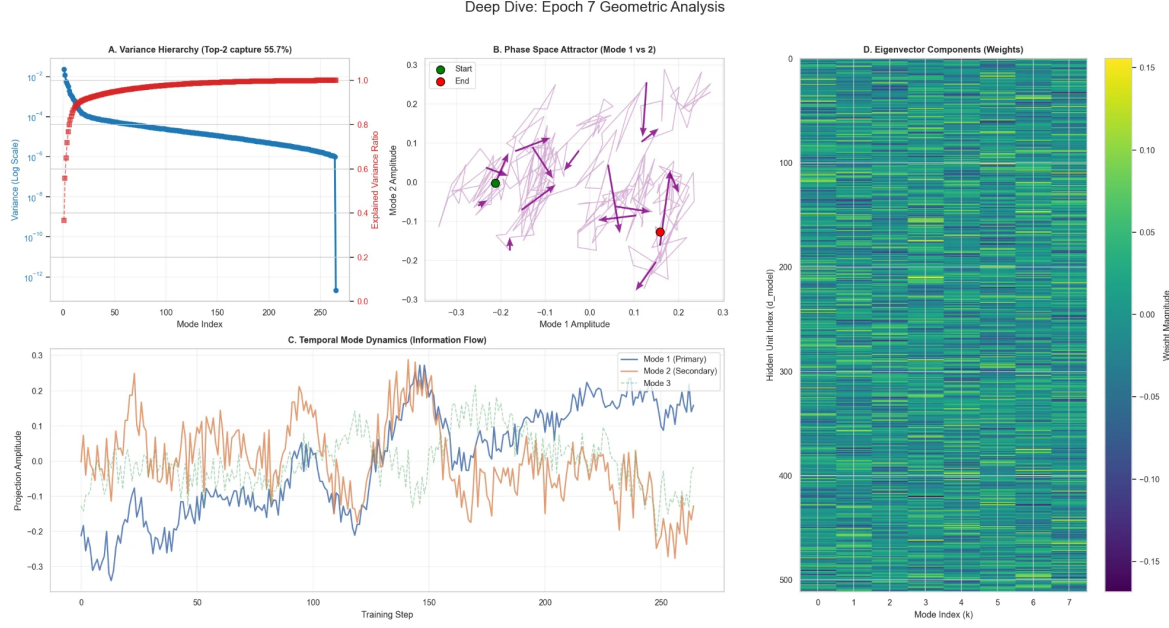
1. **Centering**: $\tilde{H} = H - \bar{h}$ where \bar{h} is the temporal mean.
2. **SVD Decomposition**: $\tilde{H} = U\Sigma V^\top$, yielding singular values σ_k and right singular vectors v_k .
3. **Variance Extraction**: Eigenvalues $\lambda_k = \sigma_k^2/(T-1)$ represent variance along each principal direction.
4. **Phase Space Projection**: Project trajectories onto top- k modes to visualize attractor geometry.

K.2 Evidence for Dimensionality Collapse

Figure 11 presents the geometric analysis for Epochs 1 and 7, revealing the evolution of the learned representation.



(a) Epoch 1: Initial attractor formation. Top-2 modes capture 69.7% of variance.



(b) Epoch 7: Refined attractor geometry. Complex oscillatory structure in phase space.

Figure 11: Geometric evolution across training. **Panel A:** Variance hierarchy showing power-law decay—the model compresses 512 dimensions into $\sim 10\text{-}20$ effective dimensions. **Panel B:** Phase space attractor showing trajectory flow. **Panel C:** Temporal mode dynamics. **Panel D:** Eigenvector structure across hidden units.

Key Observation: Rank Collapse. In every epoch, Panel A shows steep power-law decay in eigenvalues, with the cumulative variance curve reaching $\sim 100\%$ within the first 20 modes. This confirms that Spectral Memory successfully compresses the high-dimensional dynamics ($d = 512$) onto a low-rank manifold (rank $\approx 10-20$). The model learns a simplified geometric rule rather than memorizing noise.

Phase Space Evolution. Comparing Panels B between epochs reveals qualitative changes in attractor geometry:

- **Epoch 1:** Smooth, approximately linear trajectory indicating initial feature discovery.
- **Epoch 7:** Complex curved “hook” structure with clear directional flow, indicating the model has learned a specific non-linear temporal pattern that it traverses during prediction.

K.3 Subspace Stability and Geometric Convergence

The most striking evidence for geometric learning comes from analyzing how the principal subspace evolves across epochs. We compute the cosine similarity between the top eigenvector $v_1^{(e)}$ at each epoch:

$$S_{e,e'} = \left| \frac{\langle v_1^{(e)}, v_1^{(e')} \rangle}{\|v_1^{(e)}\| \|v_1^{(e')}\|} \right| \quad (52)$$

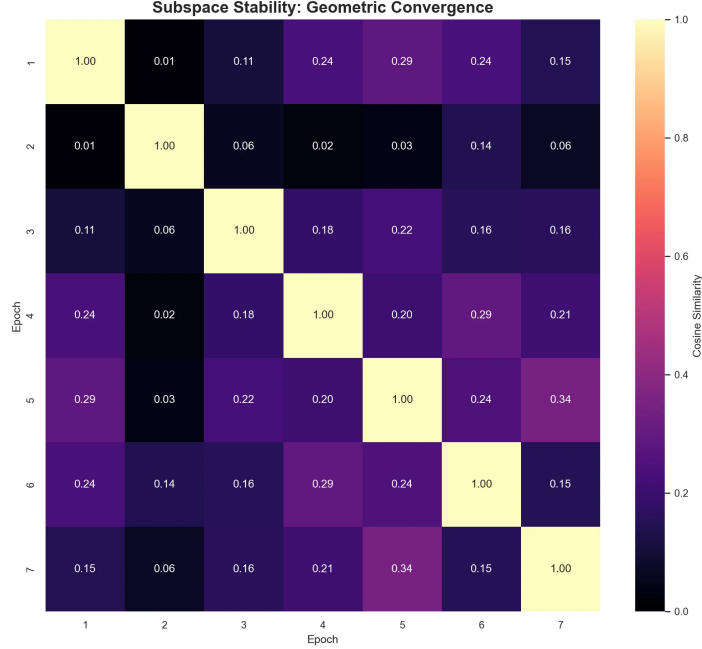


Figure 12: Subspace stability map showing cosine similarity between the primary eigenvector across epochs. Low off-diagonal values indicate continuous subspace rotation—the model explores orthogonal geometric directions during training rather than converging to a fixed attractor orientation.

Figure 12 reveals an unexpected finding: rather than converging to a fixed geometric attractor, the model exhibits **continuous subspace rotation** throughout training. Off-diagonal similarities remain low (< 0.35 for most epoch pairs), indicating that the principal direction changes substantially between epochs.

Interpretation. This behavior is consistent with the spectral filtering interpretation of Karhunen-Loëve memory. The model does not learn a single fixed manifold but rather *sculpts* the representational geometry through progressive refinement, isolating different frequency bands at different training stages. The consistent rank collapse (Panel A) combined with rotating subspace orientation suggests the model maintains a low-dimensional structure while exploring the space of possible geometric configurations.

K.4 Three-Phase Learning Trajectory

Tracking the variance captured by the top-2 modes across epochs reveals a characteristic three-phase pattern:

Phase	Epochs	Top-2 Variance
Initial Collapse	1	69.7%
Exploration	2–3	18.3% → 27.0%
Reconvergence	4–7	36.6% → 55.7%

1. **Initial Collapse (Epoch 1):** The model rapidly concentrates 69.7% of variance into two modes, discovering a strong initial attractor aligned with dominant input frequencies.
2. **Exploration Phase (Epochs 2–3):** Variance disperses dramatically (down to 18.3%), indicating the model is “breaking symmetry” to escape the initial configuration. Phase space trajectories become more chaotic during this phase.
3. **Reconvergence (Epochs 4–7):** Variance gradually reconcentrates (36.6% → 55.7%) into a refined low-rank manifold. Phase space shows structured oscillatory attractors with clear directional flow.

This trajectory mirrors classical optimization dynamics: rapid initial progress, followed by exploration of the loss landscape, culminating in convergence to a refined solution.

K.5 Manifold Alignment Visualization

To provide a global view of the representational geometry, we apply MARBLE [28] to embed the hidden state trajectories from all epochs into a shared 3-dimensional latent space. This geometric deep learning approach constructs a k -nearest-neighbor graph over temporal hidden states and learns an embedding that preserves both local geometry and vector field structure.

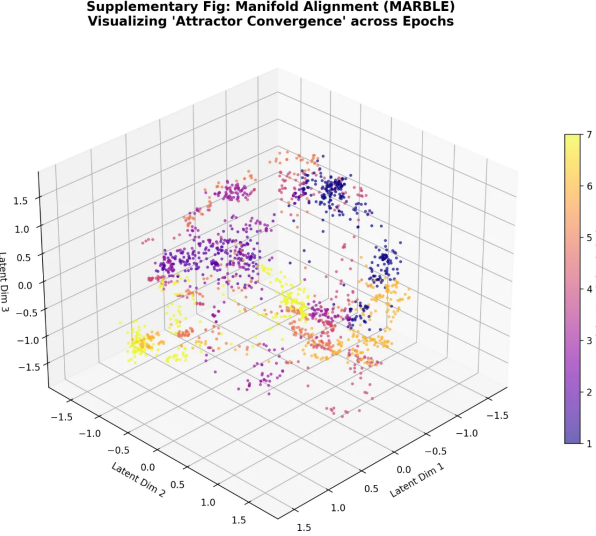


Figure 13: MARBLE manifold embedding of Spectral Memory hidden states across training epochs. Each point represents a hidden state vector, colored by training epoch (purple = epoch 1, yellow = epoch 7). The embedding reveals epoch-dependent stratification: early epochs occupy distinct regions from late epochs, with a curved trajectory connecting them. This provides evidence that training dynamics evolve along a low-dimensional manifold rather than exploring the full ambient space randomly.

Figure 13 reveals several properties of the learned geometry:

- **Epoch Stratification:** Early epochs (purple/blue) cluster in distinct regions from late epochs (orange/yellow), indicating systematic geometric evolution during training.
- **Curved Trajectory:** The transition from early to late epochs follows a curved path through the embedding space, suggesting the representational manifold has intrinsic curvature rather than being a simple linear subspace.
- **Partial Overlap:** Epochs show some intermixing in central regions, consistent with the subspace rotation observed in Figure 12—the model explores related but distinct geometric configurations.

This visualization complements the per-epoch SVD analysis by showing that the geometric evolution is globally coherent: training does not jump randomly between configurations but traces a continuous path through representation space.

K.6 Summary: Geometric Regularization in Action

The hidden state analysis provides direct empirical evidence for two central claims:

1. **Dimensionality Collapse:** The Spectral Memory mechanism forces hidden states to collapse onto a predictable low-rank manifold (effective dimension < 20), regardless of the ambient dimension ($d = 512$). This validates the theoretical connection to Karhunen-Loève expansion, where stochastic dynamics are optimally captured by a truncated set of orthogonal eigenfunctions.
2. **Dynamic Geometric Optimization:** Rather than converging to a fixed attractor, the model continuously refines its geometric representation through subspace rotation. This suggests Spectral Memory acts as a *geometric regularizer* that constrains the rank of the representation while allowing flexibility in the specific directions utilized.

These findings complement the hyperparameter scaling analysis (Appendix J) by revealing the internal mechanism through which capacity constraints translate into generalization: the (M, K) parameters control the spectral bandwidth of the learned manifold, and training dynamics naturally discover the optimal geometric configuration within these constraints.